Chloride binding in Portland composite cements containing metakaolin and silica fume

(article starts on next page)

Chloride binding in Portland composite cements containing metakaolin and silica fume

Arezou Babaahmadi [a,*], Alisa Machner [b], Wolfgang Kunther [c], João Figueira [d], Petter Hemstad [e], Klaartje De Weerdt [e]

[a] *Chalmers University of Technology, Department of Architecture and Civil Engineering, SE-41296 Gotenburg, Sweden*
[b] *Technical University of Munich, TUM School of Engineering and Design, Department of Materials Engineering, Professorship for Mineral Construction Materials, Franz-Langinger-Straße 10, 81245 Munich, Germany*
[c] *Technical University of Denmark, Department of Environmental and Resource Engineering, Brovej, 2800 Kongens Lyngby, Denmark*
[d] *Department of Chemistry, Scilife Lab, Umeå University, 90187 Umeå, Sweden*
[e] *Norwegian University of Science and Technology, NTNU, Department of Structural Engineering, Richard Birkelandsvei 1A, 7491 Trondheim, Norway*

ARTICLE INFO

ABSTRACT

This paper investigates how the composition of Portland composite cements affects their chloride-binding properties. Hydrated cement pastes prepared with a reference Portland cement and composite Portland cements containing metakaolin and/or silica fume were exposed to NaCl or $CaCl_2$ solutions. Chloride-binding isotherms were determined and the hydrate assemblage was investigated using TGA, XRD, ^{27}Al NMR, ^{29}Si NMR and thermodynamic modelling. Compared to the reference Portland cement paste, silica fume replacement did not alter the chloride-binding capacity. The metakaolin replacement resulted in the highest chloride-binding capacity. When combining silica fume with metakaolin, the chloride binding is similar to the reference Portland cement. In this study the differences in chloride binding were linked not only to changes in the AFm content, but also to alterations in the Al-uptake and chain length of the C(-A)-S-H.

1. Introduction

It is well-established that the CO_2 footprint of concrete can be decreased by replacing part of the Portland cement (PC) in concrete with suitable supplementary cementitious materials (SCMs) in the right proportions [1]. Besides the CO_2 footprint associated with cement production, one also must consider the durability of the resulting concrete elements within the framework of sustainability. It is important that additional maintenance and repair are avoided through the correct use of SCMs in concrete. One of the major degradation mechanisms for reinforced concrete is reinforcement corrosion, with chloride-induced corrosion being one of the main causes. Corrosion causes damages, which cost worldwide 3–4 % of the Growth Domestic Products, and a high portion of these costs is related to chloride-induced corrosion of the reinforcement in concrete structures [2,3].

When cementitious materials are exposed to chlorides originating from seawater or de-icing salts, some of the chlorides are chemically bound by hydration products such as Friedel's or Kuzel's salt, while other chloride ion fractions may be adsorbed on the surfaces of hydration products, such as calcium aluminosilicate hydrates (C(-A)-S-H). This is often described as physical binding, whereas the other chlorides remain free in the pore solution [4].

Over the past few decades, several researchers have reported on chemical and physical binding in hydrated cementitious materials [4–15]. Evidence that C-S-H or C(-A)-S-H can bind chloride ions has been reported in many published studies [12,15–18]. Tang and Nilsson [12] investigated the chloride-binding capacity of C(-A)-S-H in Portland cement pastes at different chloride concentrations and developed equations to fit the binding isotherms. De Weerdt et al. [4] also reported that the pH of the solution in contact with hydrated binders, plus the cations associated with chlorides, play an important role in chloride binding in hydrated cementitious systems. A decrease in the pH upon exposure to $CaCl_2$ solution has been shown to increase the total amounts of bound chlorides [4,18–21]. It has also been reported that a lowered pH in the exposure solution causes higher physical binding potential [21]. Further, it has been demonstrated that binders with lowered Ca/Si ratios, C(-A)-S-H bind less Cl than binders with a high Ca/Si ratio [22].

The use of SCMs can lead to superior resistance to chloride ingress,

---

* Corresponding author.
E-mail address: arezou.ahmadi@chalmers.se (A. Babaahmadi).

compared to conventional Portland cement [7]. It has been shown that SCMs, especially those with higher alumina content (such as fly ash, slag or metakaolin) increase the chloride-binding capacity of the cement paste [14,15,19,23–26]. However, the role of alumina in chloride binding is still unclear. While the effect of AFm phases on chloride binding is relatively well described in the literature [5,27], the effect of SCMs on the structure of C(-A)-S-H and further on the interaction of C (-A)-S-H with chloride ions is not yet fully understood. Not only do many SCMs have a higher aluminium content compared to Portland cement, they also have a higher silicon content. The increased quantities of both elements affect the structure and amount of C-S-H or C(-A)-S-H.

The objective of this study is to investigate the impact of the phase assemblage and changes in C(-A)-S-H composition, caused by varying the aluminium and silicon content in the system through the addition of SCMs, on the chemical and physical chloride-binding characteristics of the resulting hydrated pastes. This will aid a better understanding of the contribution of AFm and C(-A)-S-H to chemical and physical chloride binding. The binder systems considered in this study consist of two binary blends, incorporating 15 wt% silica fume or 15 wt% metakaolin and one ternary blend, incorporating 15 wt% silica fume and 15 wt% metakaolin. These are all compared to a plain Portland cement system. The chosen constitution amounts are meant to obtain tangible effects on polymerisation of C(-A)-S-H and add extra sources of aluminates to the system.

For the silica-fume blended-binder system, the focus is on the effect of changes in the structure and amount of C(-A)-S-H on physical binding. In metakaolin blended systems, the effect of a higher aluminium content on the AFm phases and C(-A)-S-H structures is investigated. The ternary system, incorporating both silica fume and metakaolin, is intended to reflect the mutual impact of changes in the structure of C(-A)-S-H on binding properties, with higher contents of both Si and Al incorporated in the structure, compared to the binary silica fume-containing binder.

For the determination of the chloride binding isotherms a similar approach was used as in [4,7,19,28–30]. Hydrated cement pastes of the four binders were prepared. The hydrated cement pastes were crushed, rehydrated and exposed to water, NaCl or CaCl$_2$ solutions and left to equilibrate. After equilibration, chloride-binding isotherms were determined and the pH of the exposure solution measured. The hydrate assemblage was investigated using TGA, XRD, ^{27}Al NMR and ^{29}Si NMR for the paste samples exposed to water, 2 mol/L NaCl and 1 mol/L CaCl$_2$ solution. The experimental findings were compared with thermodynamic modelling results of these systems.

First, it was verified whether changes in the hydrate phase assemblages could be provoked using the selected binder compositions, by studying the water-exposed samples as reference. The changes in the hydrate phase assemblage upon chloride exposure were then investigated. Based on this, the authors discuss the differences seen in the chloride-binding behaviour of the four investigated binders and, depending on the binder composition and exposure solution, draw general conclusions on the contribution of the AFm and C(-A)-S-H phases to chloride binding.

2. Experimental set-up

2.1. Materials

The materials used in this study were a CEM I 52.5 R Portland cement (PC) with a calcium carbonate content of 4.7 wt%, metakaolin (MK) from Powerpozz and a silica fume suspension (SF) with a dry content of 50 ± 2.5 % wt% (product name EMSAC 500SE). The oxide composition of the materials (determined by XRF) and their specific surface areas and densities are given in Table 1.

Chloride solutions, with a chloride concentration of 4 mol/L, were prepared with deionised water and NaCl or CaCl$_2$ (EMSURE analysis grade). The solutions were further diluted to chloride concentrations of 0.25, 1 and 2 mol/L, to obtain the exposure solutions used in this study. The chloride concentrations of the mother solutions (4 mol/L solutions), plus the diluted solutions, were verified by potentiometric titration. Note that a 2 mol/L NaCl solution and a 1 mol/L CaCl$_2$ solution both have a 2 mol/L chloride concentration.

2.2. Paste preparation

The four different binders investigated in this study are shown in Table 2. Cement pastes were prepared with a water-to-binder (w/b) ratio of 0.45.

The binders were prepared in a standard Hobart mixer (5 lL volume capacity), with 300 g of the dry powder and 135 g of deionised water mixed to pastes. The mixing time was 4 min at a speed of 140 rpm. The pastes were then transferred to 50 mL plastic centrifuge tubes. The bottles were filled completely, with no remaining air. The bottles were sealed and kept in a water bath at 20 °C for 30 days. To maximise the hydration degree of the paste samples, the sample preparation presented by De Weerdt et al. [4] was followed. After 30 days of sealed curing, the cement paste was crushed with a jaw crusher into fine particles passing a 1 mm sieve. The powder was stored in 1 L polypropylene bottles with extra 35 wt% deionised water and cured for 7 days at 20 °C, while the bottles were frequently shaken. The resulting moist, hardened cement paste was hammer-crushed and stored in sealed plastic bags at 20 °C for 6 months before starting the chloride exposure.

2.2.1. Free water content of the cement paste

The free water content of the well-hydrated cement paste was found by drying the solid samples at 105 °C in a vacuum oven at −0.1 MPa, until constant mass was achieved. This is a common approximation of

Table 2

Abbreviations used for the different binders tested and their composition in [wt %]. PC stands for Portland cement, MK for metakaolin and SF for silica fume.

Abbreviation	Components [wt%]		
	PC	MK	SF
Ref	100	–	–
M	85	15	–
Si	85	–	15
SiM	70	15	15

Table 1

Oxide composition in [wt%] determined with XRF, the specific surface areas in [m^2/g] determined with Blaine or BET and the specific density in [g/cm^3] of the raw materials.

	SiO$_2$ [wt%]	Al$_2$O$_3$ [wt%]	Fe$_2$O$_3$ [wt%]	CaO [wt%]	MgO [wt%]	SO$_3$ [wt%]	K$_2$O [wt%]	Na$_2$O [wt%]	SUM oxides [wt%]	LOI [wt%]	Specific surface [m^2/g]	Specific density [g/cm^3]
PC	21.39	3.69	1.29	64.66	0.72	3.43	0.57	0.21	95.96	4	0.548[a]	3.15
MK	51.89	44.83	0.42	0.02	0.05	0.03	0.12	0.22	97.58	0.83	15[b]	2.7
SF	96	–	0.1	1	0.02	0.05	–	–	97.17	4	15[b]	2.2

[a] Determined with Blaine.

[b] Determined with BET.

the free water content, even though hydration phases such as ettringite and C(-A)-S-H are also known to lose water at these conditions. The free water content of the well-hydrated binders in this study is presented in Table 3.

3. Methods

3.1. Exposing pastes to NaCl and CaCl₂ solutions

For the chloride exposure, 20 g of the well-hydrated cement paste of each binder was weighed into 50 mL plastic centrifuge tubes and 20 mL of chloride solution was added. Samples were also prepared for exposure to 20 mL of deionised water for each binder. All exposed samples were stored at 20 °C for approximately 1.5 months to reach equilibrium. During this time, the samples were shaken regularly.

It should be noted that addition of the exposure solution causes a dilution of the pore solution and thereby a reduction in the pH of the liquid phase during the exposure. This reduced pH will impact the amount of bound chlorides to some extent as reported in literature [6,26,29].

3.2. Liquid analyses

The liquid phase was extracted by centrifuging the 50 mL tubes in an XC50S3 Bio Lion centrifuge at 4000 rpm for 2 min. The resulting supernatant was removed by pipette. For each sample, the chloride concentration in solution was determined by titration, the pH was determined via a calibrated pH electrode and the elemental composition was determined by inductively coupled plasma- Atomic Emission Spectroscopy (ICP-AES). The ICP-AES measurements were conducted using an ICP-AES spectrometer with radial view manufactured by Agilent. The aqueous samples were acidified using nitric (HNO₃) acid of 69 % purity (Suprapur) from Merck. 0.02 ml of HNO₃ was added to 1 ml of the samples. The analysed elements included Ca, Na, K, S and Al and their lower quantification limits were 0.1 mg/L for Ca and Na, 0.5 mg/L for K and S, as well as 0.01 mg/L for Al.

3.2.1. Determination of the bound chloride content

To determine the chloride-binding isotherms, the chloride concentration in the clear supernatant was determined by potentiometric titration against a 0.1 M AgNO₃ solution (supplied by Honeywell Fluka), using a 916 Ti-Touch titrator from Metrohm. Depending on the concentration, 0.2–1 mL of the supernatant of each sample was pipetted into measurement beakers with 20 mL deionised water, 1 mL HNO₃ (65 %, diluted 1:10, supplied by Merck) and 2 mL 0.2 % polyvinyl alcohol (supplied by Merck).

The chloride concentration, $C_{Cl, initial}$ in [mol/L] was estimated according to Eq. (1).

$$C_{Cl, initial} = \frac{C_{Cl} \times V_{Cl}}{V_{Cl} + V_{H2O}} \qquad (1)$$

with C_{Cl} = concentration of chloride in chloride solution in [mol/L], V_{Cl} = added volume of chloride solution in ml, V_{H_2O} = water content in the sample in ml, accounted for according to the values presented in Table 3.

The calculated values of $C_{Cl, initial}$ depend on the measured free water contents. Thus, to assure the accuracy of the obtained values, the initial chloride concentrations were also measured and compared with the calculated values. The results are very similar, see appended data. The

measurements were made directly upon exposure (adding solution, shaking for 30 s followed by 2 min of centrifuging).

The concentration was then measured every week until equilibrium was achieved (1.5 months) and the equilibrium concentration in the liquid phase could be measured, $C_{Cl, equilibrium}$ in [mol/L]. The total bound chloride content, $C_{Cl, total bound}$, in [g/g dry cement paste] was calculated according to Eq. (2).

$$C_{Cl,total bound} = \frac{M_{Cl} \times \left(C_{Cl,initial} - C_{Cl,equilibrium}\right) \times \left(V_{H_2O} + V_{Cl,added}\right)/1,000}{\left(m_{sample} - m_{H_2O}\right)}$$
$$(2)$$

with $M_{Cl} = 35.45$ g/mol, the molar mass of chlorine, $V_{Cl, added} = 20$ mL, the amount of chloride solution added, $m_{sample} = 20$ g, the mass of cement paste, $V_{H_2O} = m_{H_2O}$, the amount of free water in the paste in [mL] or [g] (assuming a density of 1 g/cm³). The values are presented in Table 3. The total amounts of bound chlorides are therefore reported in [g/g dry binder at 105°C].

3.2.2. pH measurements

The pH measurements were conducted using a 6.0255.100 Profit-rode from Metrohm at 20 °C. The electrode was calibrated daily with buffer solutions of pH 7, 10 and 13. The measurements were taken by extracting 2 mL of the exposure solution into a separate 15 mL centrifuge tube. The pH was measured in this tube, which allowed for the solution to fully cover the electrode. The determination of the pH was not repeated so all reported results relate to single measurements. A typical error for pH determination in the relevant range is about 0.07 pH [31].

3.3. Solid analyses

The solids of the hydrated cement pastes exposed to water (H₂O), 2 mol/L NaCl solution (NaCl) and 1 mol/L CaCl₂ solution (CaCl₂) were investigated at equilibrium.

3.3.1. Sample preparation

About 2–3 spatulas of the solids were extracted from each of the centrifuge tubes and put through a double-solvent exchange procedure. The wet solids were placed in a 125 mL plastic bottle with 100 mL isopropanol (supplied by VWR Chemicals). The bottles were shaken for 30 s before resting for 5 min. After resting, the liquid was decanted off and another 100 mL isopropanol was added. The bottles were shaken again for 30 s and left to rest for 5 min before the suspensions were poured into a vacuum filtration unit. They were filtrated until dry and then 20 mL ethanol (99 % purity) was added. The suspension was stirred with a glass rod for 30 s before resting for 5 min. The content was then vacuum filtrated until it appeared surface-dry and was subsequently stored in a vacuum oven at 30 °C and −0.1 MPa, for one week. Afterwards, the dried paste samples were ground to a particle size of <75 μm in a Retsch RM 200 mechanical mortar for further characterisation. The phase assemblage of the various dried and ground pastes was analysed using X-ray diffraction, thermogravimetric analysis, and nuclear magnetic resonance spectroscopy.

3.3.2. X-ray diffraction

For the powder X-ray diffraction (XRD) measurements, a Rigaku Miniflex 600 with Cu-Kα radiation and a fast 1d solid-state detector was used. The scans were conducted between 3° and 63° 2Θ with a step size of 0.02° 2Θ and a scanning speed of 4 s/step.

3.3.3. Thermogravimetric analysis

For the thermogravimetric analysis (TGA) measurements, a Mettler Toledo TGA-DSC3+ was used. Approximately 30–50 mg of the ground paste was weighed into 70 μL alumina crucibles. The samples were heated from 20 °C to 1000 °C at a rate of 10 °C/min while purging with 50 mL/min N₂. The raw data can be found as appended data. The

Table 3
Free water content of the well-hydrated cement pastes, as determined by oven-drying at 105 °C for the investigated binders in [wt% of initial mass].

	Ref	M	Si	SiM
Free water content [wt%]	34	36	36	44

decomposition of phases can be identified as mass losses in specific temperature intervals [32]: C(-A)-S-H continuously loses bound water between 40 °C and 600 °C with a large peak at around 100 °C. Ettringite decomposes near 100 °C and portlandite between 400 °C and 550 °C. AFm-phases, such as Friedel's salt, monosulphate and monocarbonate have several decomposition peaks in the ranges of 150 °C–200 °C and 250 °C–400 °C. Carbonates decompose in the range of 550 °C–800 °C. Mass losses above 800 °C are potentially caused by remaining calcium or sodium chloride [33].

The DTG curves are presented; these are the derivative of the mass loss as a function of temperature. These mass losses are used to quantify the amount of Friedel's salt and portlandite using the integration method of the DTG curve with linear background subtraction, as described in [32]. The results are reported in [*wt. % per dry mass at* $800^{\circ}C$]. The measured bound water content at 800 °C, with respect to the type of binder system and exposure solution, is presented in Table 4.

The amount of portlandite in the paste, CH in [*wt. % per dry mass at* $800^{\circ}C$], was calculated according to Eq. (3).

$$CH = \frac{M_{CH}}{M_H} \times m_{CH} = \frac{74 \ g/mol}{18 \ g/mol} \times m_{CH} \qquad (3)$$

where m_{CH} is the mass loss related to the decomposition of portlandite [*wt. % per dry mass at* $800^{\circ}C$], $M_{CH} = 74 \ g/mol$, the molar mass of portlandite, and $M_H = 18 \ g/mol$, the molar mass of water.

The amount of chloride-containing AFm (Cl-AFm), which for the sake of simplicity is referred to here as Friedel's salt, FS in [*wt. % per dry mass at* $800^{\circ}C$], was calculated according to [23,34] using Eq. (4), assuming that the measured mass loss, m_{H_Fs} in [*wt. % per dry mass at* $800^{\circ}C$], relates to the 6 molecules of main layer water in the Friedel's salt structure. The m_{H_Fs} is the integrated mass loss in the temperature range of approx. 250 °C–400 °C (see appended data for the exact integration limits).

$$FS = \frac{M_{FS}}{(6 \times M_H)} \times m_{H\_FS} = \frac{561 \ g/mol}{(6 \times 18 \ g/mol)} \times m_{H\_FS} \qquad (4)$$

with $M_{Fs} = 561 \ g/mol$, the molar mass of Friedel's salt with the chemical composition of $Ca_4Al_2Cl_2(OH)_{12} \cdot 4H_2O$ or $C_3A.CaCl_2.10H_2O$ using the cement chemist notation. It should be noted, that assuming the Friedel's salt to have a Cl/Al ratio of 1 is a simplification, as Friedel's salt can occur as solid solution with for example monocarbonate [5,27]. The composition of the chloride-containing AFm was not verified in the current study.

It should be noted that if hydrotalcite is formed in the cement paste, its mass loss will partly overlap with the mass-loss peak of Cl-AFm as they appear in the same temperature range [30]. However, in the investigated pastes exposed to water, no mass loss of hydrotalcite could be observed via the method used. This indicates that the overlap between hydrotalcite and Cl-AFm is not an issue for the samples investigated in this study.

The quantification of CH and FS was not repeated so all reported results relate to single measurements. In [35] a similar method was used for determination of the CH content and a standard deviation of 0.2 wt% determined on triplet samples was reported.

Table 4
Bound water content at 800 °C determined by TGA measurements in [wt% of initial mass], with respect to the type of binder system and the exposure solution.

Exposure solution	Bound water content at 800 °C [wt% of initial mass]			
	Ref	M	Si	SiM
NaCl	29.3017	30.4957	29.4146	30.8052
CaCl₂	30.6053	31.5135	30.059	32.5516

3.3.4. Nuclear magnetic resonance spectroscopy

The silicon and aluminium coordination in the hydrated, water and chloride-exposed pastes were measured by ^{29}Si and ^{27}Al solid-state nuclear magnetic resonance spectroscopy (NMR), to investigate the changes in the C(-A)-S-H structure. Both the ^{29}Si and ^{27}Al MAS NMR spectra were obtained using a Bruker 4 mm MAS BB/^1H probe at 298 K. Samples were packed in 4 mm zirconia rotors. The ^{29}Si high-powered decoupled (HPDEC) MAS NMR spectra were acquired at 2500 scans at a spin rate of 7.5 kHz. This used a 3 μs pulse, corresponding to an excitation angle of about 45° and a relaxation delay of 30 s. The ^{27}Al HPDEC MAS NMR used a total of 2048 scans at a spin rate of 11 kHz, using a 4 μs pulse corresponding to an excitation angle of about 65° and a relaxation delay of 0.8 s. Both experiments used SPINAL64 proton decoupling with a ^1H-field strength of 50 kHz [36]. The intensities of each ^{29}Si spectra are normalized with consideration of total intensities in relation to the reference spectrum; Ref cement exposed to water. The Mean aluminosilicate change lengths (CL), the average chain length of pure silica units (CL Si) and the average molar Al/Si ratio for Al incorporated into the silicate chains of the C(-A)–S–H structure were calculated, based on the ^{29}Si NMR results according to Richardson et al. [37] as well as Richardson and Groves [38].

3.4. Thermodynamic modelling

The Gibbs free energy minimisation software, GEMS v.3.7 [39,40], was used to model the changes in the hydrate phase assemblage in the samples upon exposure to water and 2 mol/L NaCl or 1 M CaCl₂ solution at 20 °C. A cement-specific database (CEMDATA18) [41] containing solubility products of cementitious materials was used, in combination with the PSI/Nagra Chemical Thermodynamic Database. The XRF-results of the raw materials were used as input for the composition of the binders investigated in the model. Several phases were excluded from the model, as their formation is unlikely for the exposure conditions: gibbsite, kaolinite, thaumasite, hematite, magnetite, brucite and quartz. The formation of siliceous Fe-hydrogarnet was enabled, while siliceous Al-Fe-hydrogarnet solid solution was excluded. The amount of mol Al per mol Si in the C(-A)-S-H was accounted for based on NMR measurements, as shown in Table 5. This amount of Al was removed from the reactive system to account for the Al-uptake of C(-A)-S-H, thereby predicting more realistic amounts of AFm phases. The model was developed so as to simulate the solid/liquid ratio of the adsorption test. However, 100 g of dry binder was assumed to react with 196 g of water, to create 196 g of paste (instead of 20 g of paste used in adsorption test). The corresponding exposure solution quantities, 196 ml of 2 mol/L NaCl or 1 mol/L CaCl₂ solution were added to the system (instead of 20 ml used in adsorption tests).

The following assumptions were made in the model:

- Degree of reaction (DoR) of PC is 100 % for all binders.
- DoR of SF is 40 % for the Si and SiM binders.
- DoR of MK is 50 % for the M and SiM binders.
- Physical chloride binding by the C(-A)-S-H was not considered in the model.

The degree of reaction (DoR) of the SCMs were roughly estimated based on their portlandite consumption, assuming a DoR of the Portland cement of 100 %. Therefore, the DoR of the SCMs as input in the GEMS model was adjusted so that the portlandite content predicted by GEMS would approx. match the portlandite content measured experimentally by TGA. The suggested levels of the DoR of the SCMs agree with literature. According to Skibsted and Snellings [42], for a clinker substitution of 30–50 % of metakaolin, a DoR in the range of approximately 35–45 % can be expected for metakaolin, whereas for silica fume, a DoR of up to 60 % was reported by Muller et al. [43] for a 10 % substitution.

The effect of the Al-uptake in the C(-A)-S-H was not taken into account when the portlandite contents were matched. Thus, when the Al-

Table 5
Summary of the main differences in phase assemblage of the water (H2O), NaCl and CaCl2 solution-exposed paste samples. The M, Si and SiM binder's pastes are compared to the Portland cement paste reference samples (Ref) exposed to water. The amount of AFm, AFt and C(-A)-S-H is obtained by thermodynamic modelling. The chain length (CL), silica chain length (CL Si) and Al/Si molar ratio of C(-A)-S-H is determined by ^{29}Si NMR.

Exposure	Binder	AFm [g/100 g binder][a]	AFt [g/100 g binder][a]	C(-A)-S-H [g/100 g binder][a]	C(-A)-S-H (CL) [−]	C(-A)-S-H (CL Si) [−]	C(-A)-S-H Al/Si [−]
H2O	Ref	3.0	18	75	3.6	2.5	0.10
	M	14.6	15	78	4.3	2.7	0.11
	Si	0.7	16	83	4.1	2.6	0.11
	SiM	7.0	13	83	6.5	3.0	0.16
NaCl	Ref	3.8	18	74	4.0	2.8	0.09
	M	14.6	15	77	5.4	3.1	0.11
	Si	4.0	16	82	4.5	3.1	0.08
	SiM	9.3	13	82	8.7	3.8	0.13
CaCl2	Ref	4.5	18	75	3.4	2.5	0.08
	M	16.5	15	77	3.4	2.5	0.09
	Si	5.5	16	82	3.2	2.6	0.06
	SiM	10.4	13	82	6.2	3.2	0.13

[a] Predicted by thermodynamic modelling.

uptake in C(-A)-S-H is accounted for, less AFm is formed, therefore more calcium is available to form portlandite. GEMS therefore overestimates the portlandite content when compared to experimental results. The thermodynamic modelling does not predict a change in Ca/Si ratio of the C(-A)-S-H as long as the portlandite is present, a final refinement of the DoR of the SCMs to match the portlandite content was therefore not performed.

4. Results and discussion

4.1. Water-exposed samples

As a first step, it was determined whether considerable variation in AFm content and C(-A)-S-H structure could be obtained with the different binders used in this study. The hydrate assemblage of the various binders exposed to water (H2O) is therefore discussed as reference systems first.

4.1.1. Ref H2O

For the reference Portland cement paste (Ref) exposed to water (H2O), the thermodynamic modelling predicts the presence of C(-A)-S-H, portlandite, ettringite and some monocarbonate (see Fig. 1).

The DTG curve for Ref-H2O (Fig. 2) is in line with these predictions, as they indicate the presence of ettringite and C(-A)-S-H with the main peak at about 120 °C, followed by a shoulder just below 200 °C and two smaller ones at about 300 °C and just below 400 °C. These correspond to AFm and a very clear portlandite peak between 400 and 500 °C. The portlandite content predicted by thermodynamic modelling and the amount determined by TGA show similar trends (Fig. 3). The observed differences between the predicted and measured data can be expected as described in the description of the thermodynamic model (Section 3.4).

The presence of ettringite and monocarbonate was confirmed experimentally by the XRD spectra for the Ref H2O sample in Fig. 4. The ^{27}Al NMR spectrum for Ref-H2O in Fig. 5 also indicates the presence of AFm and AFt phases.

The normalized ^{29}Si NMR spectrum related to the C(-A)-S-H of the Ref-H2O sample (Fig. 6) shows a larger peak related to silicon tetrahedra in Q^1 coordination, and a smaller peak for Q^2 coordinated silicon and a small shoulder in the Q^2(Al) region. The average chain length (calculated based on the ^{29}Si NMR spectrum) is 3.6 and the silicate chain length is 2.5 (Fig. 7). The Al/Si molar ratio of the C(-A)-S-H is 0.10 (Fig. 8), which is slightly higher than the values reported in the literature for similar systems [35,44]. Q^3 and Q^4 intensities are not observable in the ^{29}Si spectra (< −90 ppm; see also Fig. 16 in Appendix A with extended ppm range), which could indicate the consumption of the SCMs or be artifact related to the relaxation state of the silica in SF. However, the full consumption of the SCMs would have led to a depletion of all portlandite in the modelling for all SCM containing binders. Hence, the DoR were reduced for SF and MK to account for the observed phase assemblages from XRD and TGA as described in Section 3.4.
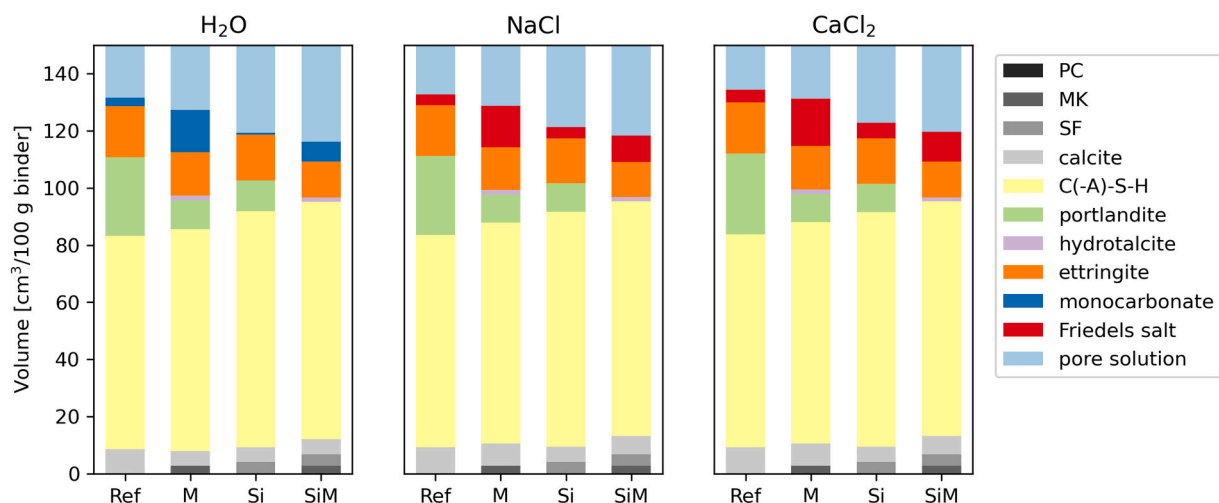
Fig. 1. The phase assemblage predicted by GEMS for the Ref, M, Si and SiM binder's pastes exposed to water (H2O), or NaCl or CaCl2 solutions with a 2 mol/L chloride concentration.
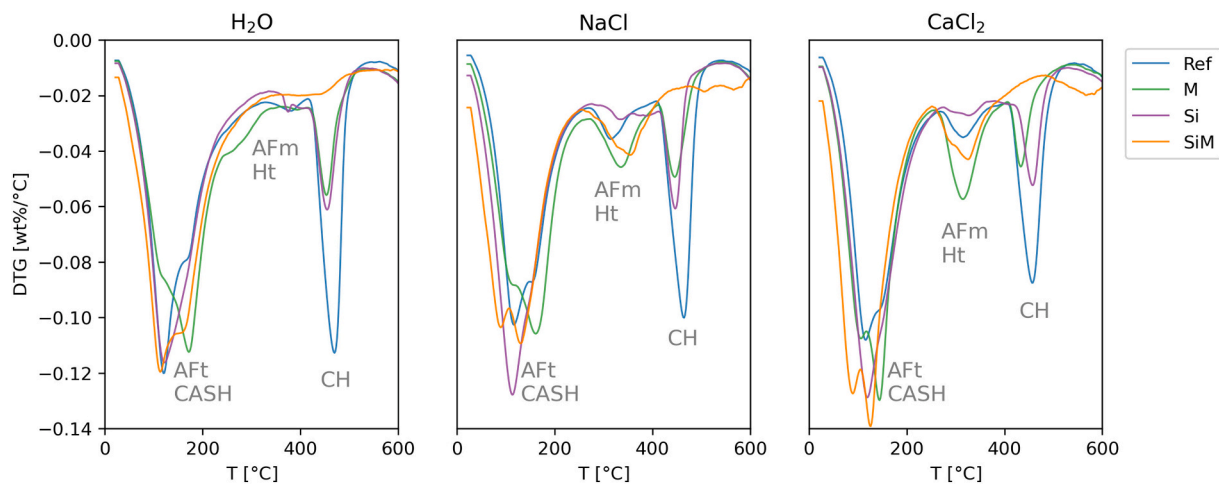
Fig. 2. DTG curves in the 50 °C to 600 °C range for the Ref, M, Si and SiM binder's pastes exposed to water (H_2O), or NaCl or $CaCl_2$ solutions with a 2 mol/L chloride concentration. The mass-loss peaks typically associated with AFt, C(-A)-S-H, AFm, hydrotalcite (Ht) and portlandite (CH) are marked.
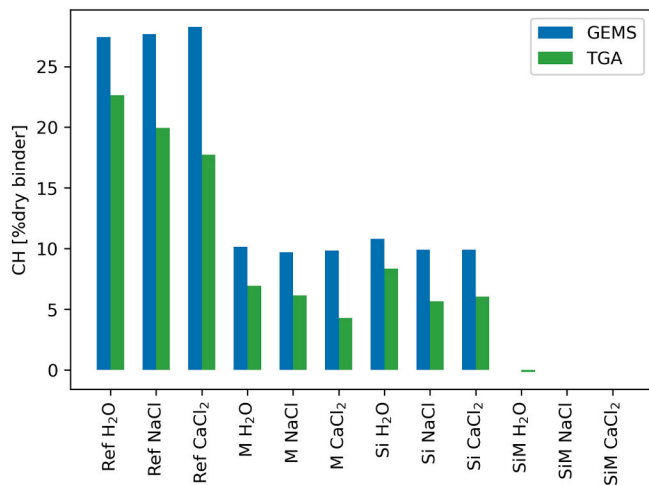

Fig. 3. Comparison of the portlandite content per dry binder predicted by GEMS and measured by TGA. The samples of SiM binders were analysed, but the CH contents were very low.

The incorporation of alumina in the C(-A)-S-H is also confirmed by the ^{27}Al NMR spectrum of the Ref-H_2O sample shown in Fig. 9. This is observed as a clear signal in the ppm range for four-fold coordinated aluminium.

4.1.2. Si H_2O

Upon replacement of 15 wt% of the PC with silica fume in the Si cement paste samples, the thermodynamic model predicts an increased amount of C(-A)-S-H, due to the pozzolanic reaction of the silica fume (Fig. 1). The pozzolanic reaction and dilution of the PC results in a lower portlandite content; approximately 10 wt%, compared to the reference Ref-H_2O with 27 wt% (Fig. 3). The amount of ettringite is reduced by approximately 11 % for the Si-H_2O paste compared to the Ref-H_2O paste, due to the dilution of PC, which is the source of the aluminates and sulphates in this system. The type of AFm phase predicted to form is monocarbonate. The predicted amount of monocarbonate in the Si paste is less than a quarter of the amount formed for the Ref-H_2O paste. This is partially due to the higher aluminium uptake by the C(-A)-S-H in the Si-H_2O paste, as the Al/Si ratio and amount of C(-A)-S-H is slightly higher compared to the Ref-H_2O paste (Fig. 7 and Table 5). As more aluminium is taken up by the C(-A)-S-H, less is available to form AFm phases. In addition, the dilution of the PC by silica fume will further contribute to a

reduction in AFm, as described for ettringite above.

The predicted decrease in portlandite, due to the pozzolanic reaction of the silica fume, was confirmed experimentally by TGA (Fig. 3). The predicted portlandite content for the Si-H_2O sample, 10 wt%, corresponds very well to the amount measured by TGA, 8 wt%. The DTG curve for the Si-H_2O sample (Fig. 2) is very similar to that of the Ref-H_2O sample, except for the less pronounced shoulder (just below 200 °C) and a smaller peak at about 300 °C, compared to the Ref-H_2O sample. This indicates a decrease in the number of AFm phases formed, which is in line with the thermodynamic modelling results.

The XRD spectrum for the Si-H_2O sample in Fig. 4 confirms the predicted formation of ettringite and monocarbonate. The peak height of monocarbonate for the Si-H_2O sample is lower compared to that of Ref-H_2O. This may be an indication of a reduction in the AFm quantity. The ^{27}Al NMR spectrum for Si-H_2O in Fig. 5 also shows a decrease in the intensity of aluminium coordinated in phases assigned as AFm and AFt phases.

The normalized ^{29}Si NMR spectrum related to the C(-A)-S-H of the Si-H_2O sample (Fig. 6) shows a similar Q^1 and a slightly higher Q^2 peaks, compared to the Ref-H_2O sample. The Q^2 peak has increased compared to the Q^1 peak. This indicates a higher degree of polymerisation of the C(-A)-S-H. Thus, one would anticipate a greater chain length for the C(-A)-S-H in the Si-H_2O sample, compared to the reference system. The calculated average chain length and Al/Si ratio, based on the ^{29}Si NMR spectrum (Fig. 7), are 4.1 and 0.11 respectively for the Si-H_2O sample, compared to the 3.6 and 0.10 for the reference. The observed increase in alumina incorporation in the C(-A)-S-H compared to the Ref-H_2O sample (as determined by ^{29}Si NMR) is probably due to the uncertainty of the method. This is because the signal for the Si-H_2O sample in the ppm range for four-fold coordinated aluminium is very similar when compared to the Ref-H_2O sample (Fig. 9).

4.1.3. M H_2O

Upon replacement of 15 wt% of the PC with metakaolin in the M cement paste samples, an increased amount of C(-A)-S-H is predicted by thermodynamic modelling, due to the pozzolanic reaction of metakaolin (see Fig. 1). The pozzolanic reaction and dilution of the PC is predicted to result in a reduced portlandite content, from about 27 wt% for the Ref-H_2O to about 10 wt% for the M-H_2O sample (Fig. 3). The amount of ettringite is reduced by approximately 15 % for the M binder's sample, compared to the Ref paste. This is due to the dilution of PC, which is the source of sulphates in the binder. The additional aluminates from the metakaolin reaction cause a four-fold increase in the predicted amount of monocarbonate, compared to the Ref-H_2O system.

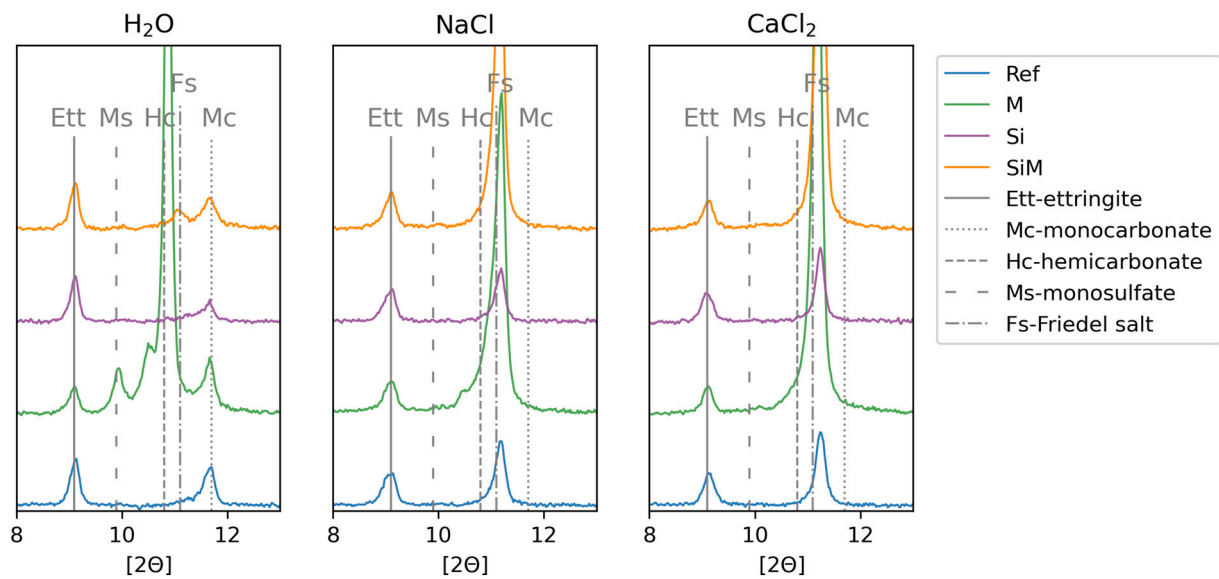The DTG curve for the M-H_2O sample (Fig. 2) shows a considerably

Fig. 4. XRD spectra, from 8 to 13 2θ showing the main AFm and AFt peaks for the Ref, M, Si and SiM binder's pastes exposed to water (H_2O), or NaCl or $CaCl_2$ solutions with 2 mol/L chloride concentration. Typical diffraction angles for ettringite (Ett), monocarbonate (Mc), hemicarbonate (Hc), monosulphate (Ms) and Friedel's salt (Fs) are indicated as a visual guide.
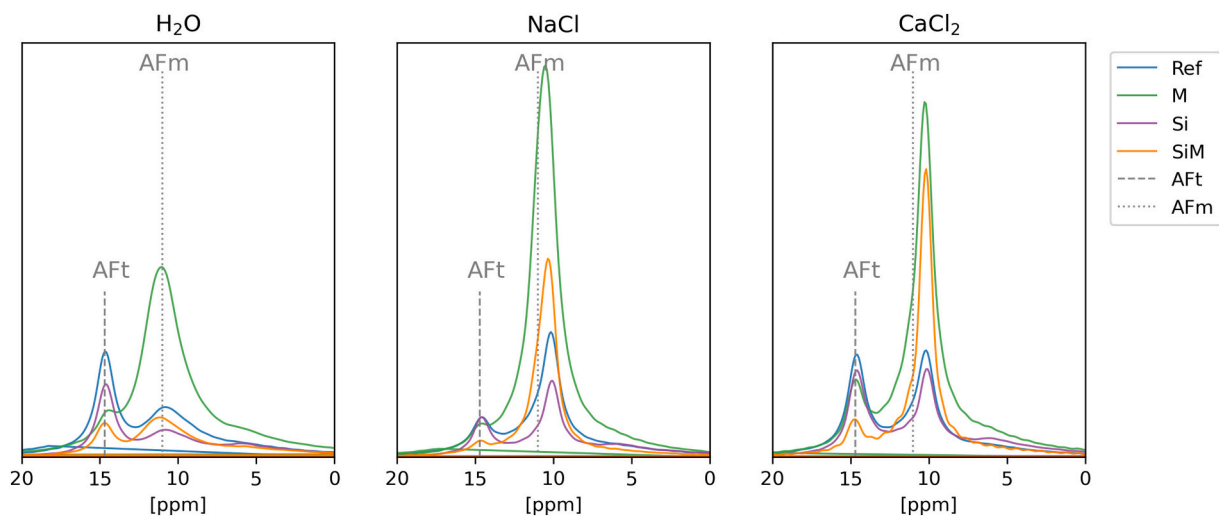

Fig. 5. ^{27}Al NMR spectra for the six-fold coordinated Al(VI) from 20 to 0 ppm which corresponds to AFm and AFt phases (indicated with lines as a visual guide). Results are shown for the Ref, M, Si and SiM binder's pastes exposed to water (H_2O), or NaCl or $CaCl_2$ solutions with a 2 mol/L chloride concentration.

larger shoulder (just below 200 °C) compared to the Ref-H_2O sample, plus a larger minor peak (at about 300 °C). This indicates an increased quantity of AFm phases formed, thereby qualitatively confirming the thermodynamic modelling. The predicted decrease in portlandite was also confirmed experimentally by TGA (Figs. 2 and 3). However, the predicted portlandite content (approximately 10 wt%) is slightly higher than the measured one (approximately 7 wt%). This might be due to a slight change in the Ca/Si ratio of the C(-A)-S-H (not accounted for in the thermodynamic model), or a different reaction degree of metakaolin compared to the assumed degree (50 wt%). The peak for the M-H_2O sample (about 120 °C) in the DTG-curve relating to C(-A)-S-H and ettringite is slightly smaller compared to the Ref-H_2O sample. This might indicate a slight decrease in the amount of ettringite.

The presence of ettringite was confirmed experimentally by the XRD spectra for the M-H_2O sample in Fig. 4. The peak height of the ettringite is lower compared to that of the Ref-H_2O sample. This might indicate a reduction in ettringite, which is in line with the observations on the DTG-curves. However, there is a difference between the type of

predicted and modelled AFm phases. This is because the XRD spectrum shows the presence of hemicarbonate and even monosulphate (as well as monocarbonate), while the thermodynamic modelling predicts monocarbonate as the only AFm phase. This discrepancy between the modelled AFm phases and those observed experimentally might be due to several mechanisms. It has been observed that the transformation of hemicarbonate to monocarbonate takes time and is dependent on the Al_2O_3/CO_2 ratio of the bulk system, which changes during hydration [35,45–48].

The ^{27}Al NMR spectrum for M-H_2O in Fig. 5 also shows a clear increase of aluminium in AFm phases and a slight decrease in the aluminium in the AFt phases. When assuming that the amount of aluminium in the AFm and AFt phases is related to the amount of these phases, the ^{27}Al NMR spectrum confirms the predicted increase in AFm and decrease in AFt by thermodynamic modelling.

The normalized ^{29}Si NMR spectrum related to the C(-A)-S-H of the M-H_2O sample (Fig. 6) is slightly different, compared to the one for the Ref-H_2O sample. The Q^1 peak is smaller and the Q^2 (Al) peak is more
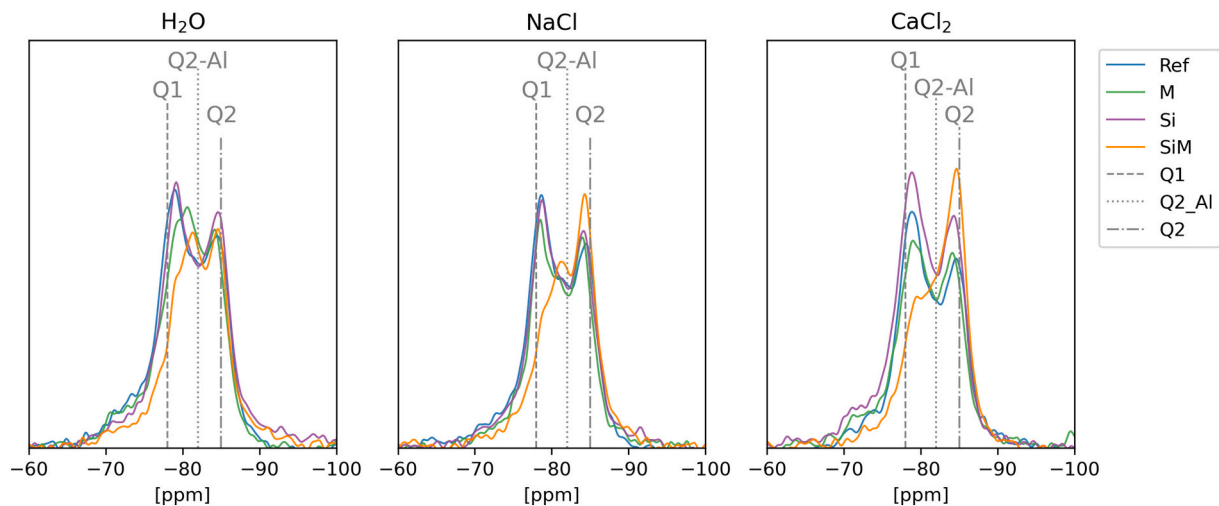
Fig. 6. Normalized ^{29}Si NMR spectra for the Ref, M, Si and SiM binder's pastes exposed to water (H_2O), or NaCl or $CaCl_2$ solutions with a 2 mol/L chloride concentration. The Q^1 (silicon end-members tetrahedron), Q^2(Al) (bridging tetrahedron connected to Al) and Q^2 (bridging tetrahedron) are indicated by lines in the figures as a visual guide.
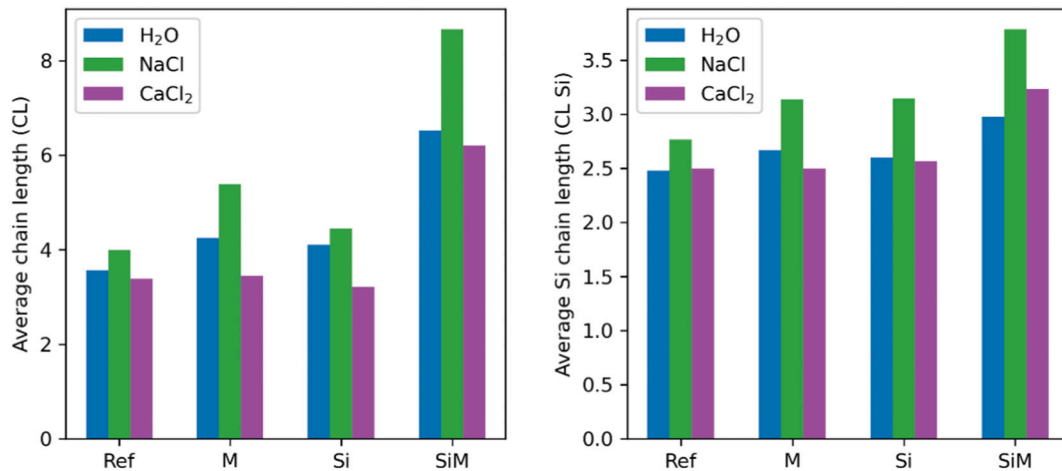
Fig. 7. The calculated average chain length (CL) and average Si chain length (CL Si) of the C(-A)-S-H based on the deconvoluted ^{29}Si NMR spectra from the Ref, M, Si and SiM binder's pastes exposed to water (H_2O), NaCl or $CaCl_2$ solutions with a 2 mol/L chloride concentration.

pronounced, indicating a higher aluminium uptake in the C(-A)-S-H. For the M-H_2O sample, the calculated average chain length and silicate chain length based on the ^{29}Si NMR spectrum are 4.3 and 2.7 respectively (see Fig. 7) and the Al/Si molar ratio of the C(-A)-S-H is 0.11 (Fig. 8). This means a slight increase in chain length and aluminium uptake in the C(-A)-S-H compared to the Ref-H_2O sample. The incorporation of more alumina in the C(-A)-S-H compared to the Ref-H_2O sample is confirmed by the ^{27}Al NMR spectrum shown in Fig. 9. This is because the signal observed in the ppm range for four-fold coordinated aluminium is higher for the M-H_2O, compared to the Ref-H_2O sample.

4.1.4. SiM H_2O

Upon replacement of 30 wt% of the PC with 15 wt% silica fume and 15 wt% metakaolin in the SiM binder's paste samples, an increased amount of C(-A)-S-H is predicted due to the pozzolanic reaction of metakaolin and silica fume (Fig. 1). The pozzolanic reaction and dilution of the PC results in full consumption of the portlandite content (Fig. 3). The amount of ettringite is reduced by approximately 30 % for the SiM binder compared to the Ref paste, as anticipated. The type of AFm phase predicted by modelling is monocarbonate and the predicted quantity is about 2.5 times higher compared to the Ref paste, as similarly described for the M binder's sample. This is due to an increase in the aluminium

content of the system.

The absence of portlandite was confirmed experimentally by TGA (Figs. 2 and 3). The DTG curve for the SiM-H_2O sample (Fig. 2) shows a considerably larger shoulder just below 200 °C compared to the Ref-H_2O sample, thereby confirming the predicted increase in the amount of AFm phases formed (Fig. 1).

The XRD spectrum for the SiM-H_2O sample in Fig. 4 confirms the predicted formation of ettringite and monocarbonate but also shows the presence of hemicarbonate. As for the M-H_2O sample, the presence of hemicarbonate instead of just monocarbonate might be due to kinetics [46–49]. The ^{27}Al NMR spectrum for SiM-H_2O sample in Fig. 5 indicates a decrease in AFt content compared to the reference and a relative increase in AFm. This is in line with the predictions of the thermodynamic modelling.

The normalized ^{29}Si NMR spectrum related to the C(-A)-S-H of the SiM-H_2O sample (Fig. 6) shows higher Q^2 and Q^2 (Al) peaks and a lower Q^1 peak compared to the Ref-H_2O sample. This indicates a greater chain length and aluminium incorporation compared to the reference. This was confirmed by the calculated average chain length and Al/Si ratio, based on the ^{29}Si NMR spectrum (Figs. 8 and 7) which were 6.5 and 0.16 respectively for the SiM-H_2O sample. The incorporation of more alumina in the C(-A)-S-H of the SiM binder's sample compared to the Ref-H_2O
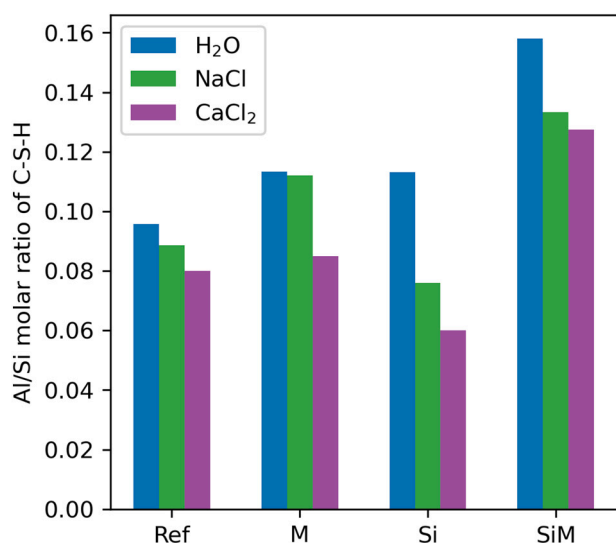
Fig. 8. Al/Si molar ratio of the C(-A)-S-H based on the deconvoluted ^{29}Si NMR spectra from the Ref, M, Si and SiM binder's pastes exposed to water (H$_2$O), NaCl or CaCl$_2$ solutions with a 2 mol/L chloride concentration.

sample is also confirmed by the ^{27}Al NMR spectrum shown in Fig. 9. This is because the signal for the SiM-H$_2$O sample in the ppm range for four-fold coordinated aluminium was much higher compared to the signal from the Ref-H$_2$O sample.

4.1.5. Summary of the difference in hydrate assemblage for the investigated binders upon water exposure

The authors were able to produce hydrated cement pastes with varying AFm contents and varying C(-A)-S-H compositions and amounts. The main differences in the phase composition, as predicted by GEMS, are summarised in Table 5. The M binder paste has a higher AFm phase content compared to the reference and SiM binder's paste. The amount of AFt is reduced in the composite binders, due to the replacement of PC, which is the sole sulphate source in the system. The amount of C(-A)-S-H increases by about 10 wt% for the paste samples of Si and SiM binders and by 4 wt% for the M binder, compared to the reference, based on thermodynamic modelling. The only binder which produced a considerable change in the C(-A)-S-H composition was the SiM binder,

which showed an increased Al/Si ratio and consequently also chain length (CL).

4.2. Chloride-exposed samples

This section aims to elucidate the impact of changes in the assemblage and composition of the various binder's key phases on the chloride-binding characteristics of the hydrated cement pastes.

4.2.1. Binding isotherms and characteristics of the exposure solutions

Fig. 10 shows the chloride-binding isotherms for the Ref, M, Si, and SiM binders that were exposed to NaCl (left) and CaCl$_2$ (right) solutions in varying concentrations. The horizontal axes show the chloride concentration of the exposure solution at equilibrium. The M binder seems able to bind the highest level of chlorides, compared to the other binders (such as Ref, Si and SiM) which appear to bind similar quantities of chlorides. More chloride binding is observed for CaCl$_2$ exposure compared to NaCl exposure, as anticipated [4,6,18–20,50–52].

The pH of the exposure solutions after equilibration is shown in Fig. 11. The pure Portland cement paste (Ref) has the highest pH compared to the other binders (M, Si and SiM) when exposed to H$_2$O, as anticipated [53,54]. For NaCl exposure, the pH of the exposure solution does not seem to vary greatly with the chloride concentration. However, a clear decrease in pH is observed for CaCl$_2$ exposure, which is in line with [4,18–21]. For the samples of Si and M binder, the decrease in the pH upon CaCl$_2$ exposure seems independent of the concentration. However, a certain concentration dependency is observed for the samples representing Ref and SiM binders.

The elemental composition of the exposure solutions after equilibration (at a chloride concentration of 2 mol/L) is shown in Fig. 12 in terms of measured and thermodynamically modelled calcium, sodium, sulphate, aluminium and potassium concentrations. The elemental composition of the exposure solutions after equilibration upon exposure to chloride concentrations lower than 2 mol/L, are provided as appended data.

The calcium concentrations in the water exposed samples as well as NaCl exposed samples are similar to the reported ranges of calcium in the pore solution in hydrated cement paste, approximately 1–10 mmol/L [53]. For the CaCl$_2$ exposed samples the modelled and measured calcium concentrations are in the range of 500 mmol/L. Measured and modelled calcium concentrations are in acceptable agreement for all exposure solutions.
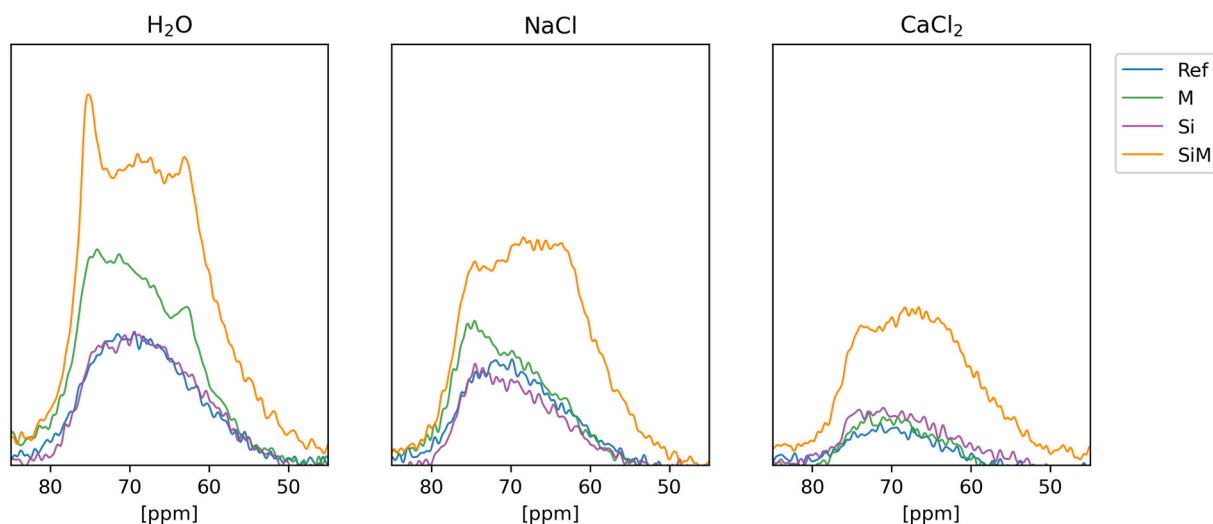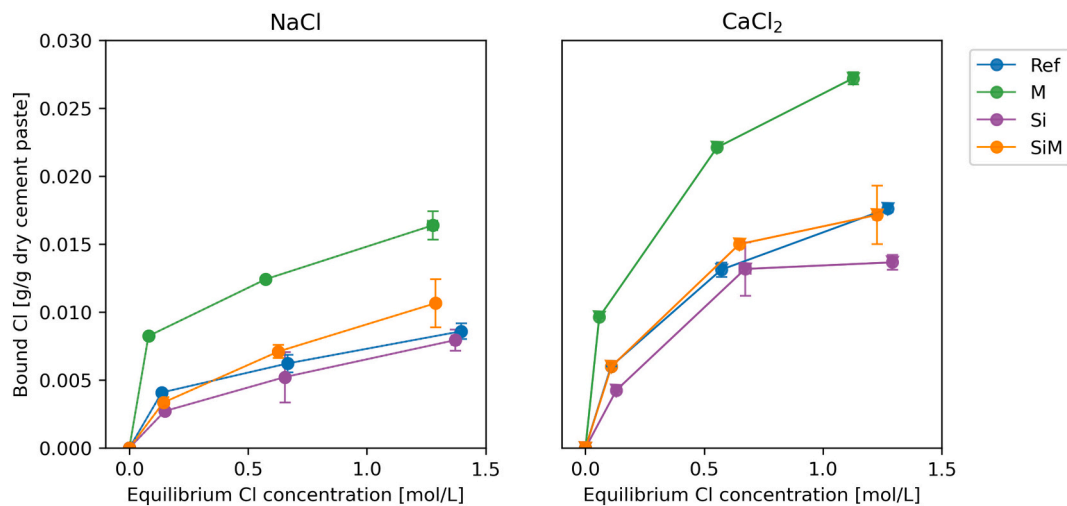

Fig. 9. ^{27}Al NMR spectra for the four-fold coordinated Al(IV) from 90 to 40 ppm which corresponds to the alumina incorporated into the C(-A)-S-H at bridging sites where aluminium replaces silica. Results are shown for the Ref, M, Si and SiM binder's pastes exposed to water (H$_2$O), or NaCl or CaCl$_2$ solutions with a 2 mol/L chloride concentration.

Fig. 10. Chloride-binding isotherms for the Ref, M, Si and SiM binder's pastes exposed to NaCl or CaCl$_2$ solution. The horizontal axes show the chloride concentration of the exposure solution at equilibrium. The samples exposed to H$_2$O are shown at 0 mol/L. All measuring points represent the average of measurements performed on duplicate samples except for the point with the highest chloride concentration where triplicates were measured. The error bars indicate standard deviation of both the bound Cl (vertical) and equilibrium concentration (horizontal).
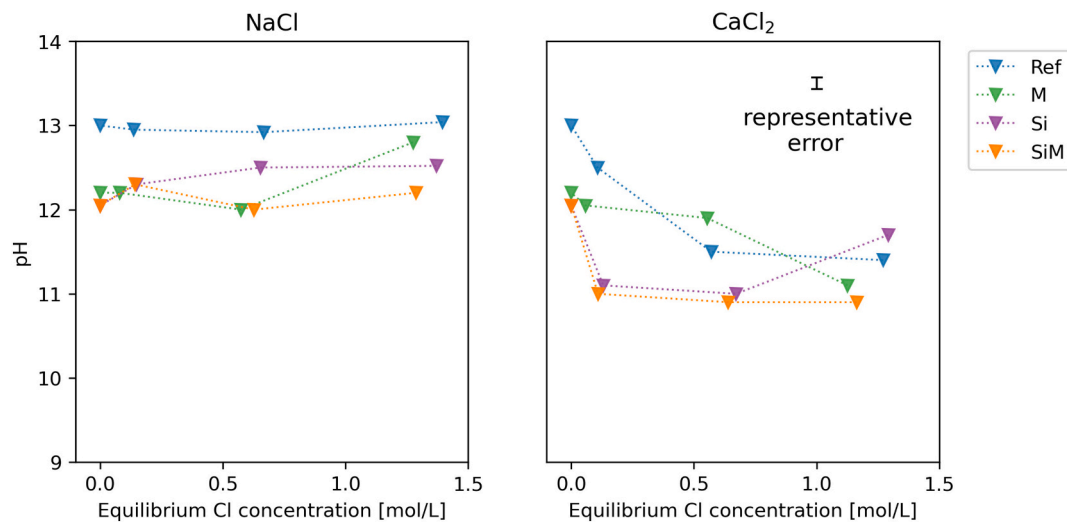
Fig. 11. The pH of the exposure solution for the Ref, M, Si and SiM binder's pastes exposed to NaCl or CaCl$_2$ solution. The horizontal axes show the equilibrium chloride concentration of the exposure solution. The samples exposed to H$_2$O are shown at 0 mol/L. A representative error of ± 0.07 pH, typical for pH measurements in this range [31], is indicated in the figure.

The sodium concentration in the water exposed samples as well as CaCl$_2$ exposed samples agrees well with the ranges of sodium concentration of pore solution in hydrated cement paste, 50–150 mmol/L, reported in the literature [53]. The reported concentrations of sodium strongly depend on the w/c ratio of the pastes and the total content of Na$_2$O of the OPC. Measured and modelled values of sodium concentration are in acceptable agreement.

The concentration of aluminium decreases upon exposure to NaCl and reaches values below the detection limits for these measurements (<0.01 ppm) when samples were exposed to CaCl$_2$ solution, although small discrepancies from this trend are seen in binder SiM. The concentration ranges of aluminium in water exposed samples, is in agreement with the reported ranges of the aluminium concentration of pore solution in hydrated cement paste, 0.001–1 mmol/L, reported in the literature [53]. Measured and modelled values of aluminium concentration are in acceptable agreement for all exposure solutions.

Sulphate concentrations tend to increase upon exposure to NaCl solution. This has been explained recently for Portland cement [5], due to

the higher stability of Cl-AFm compared to sulphate-containing AFm (S-AFm). However, the sulphate concentrations upon exposure to CaCl$_2$ are in a similar range as for samples exposed to water. Similar behaviour has previously been reported in the literature [4], and was explained by the formation of additional ettringite upon CaCl$_2$ exposure, due to the lower pH of the system. The sulphate concentration in the water exposed samples agrees with the ranges of sulphate concentration of pore solution in hydrated cement paste, 0.1–10 mmol/L, reported in the literature [53]. Measured and modelled values of sulphate concentration are in acceptable agreement in the case of all exposure solutions.

The potassium concentration seems not to be affected by exposure to chloride solutions. The measured values are in agreement with predicted ones, and with the ranges of potassium concentration of pore solution in hydrated cement paste, <700 mmol/L, reported in the literature [53]. The reported concentrations of potassium strongly depends on the w/c ratio of the pastes and the total content of K$_2$O of the OPC and for higher w/c ratios, lower potassium concentrations are observed due to dilution [53].
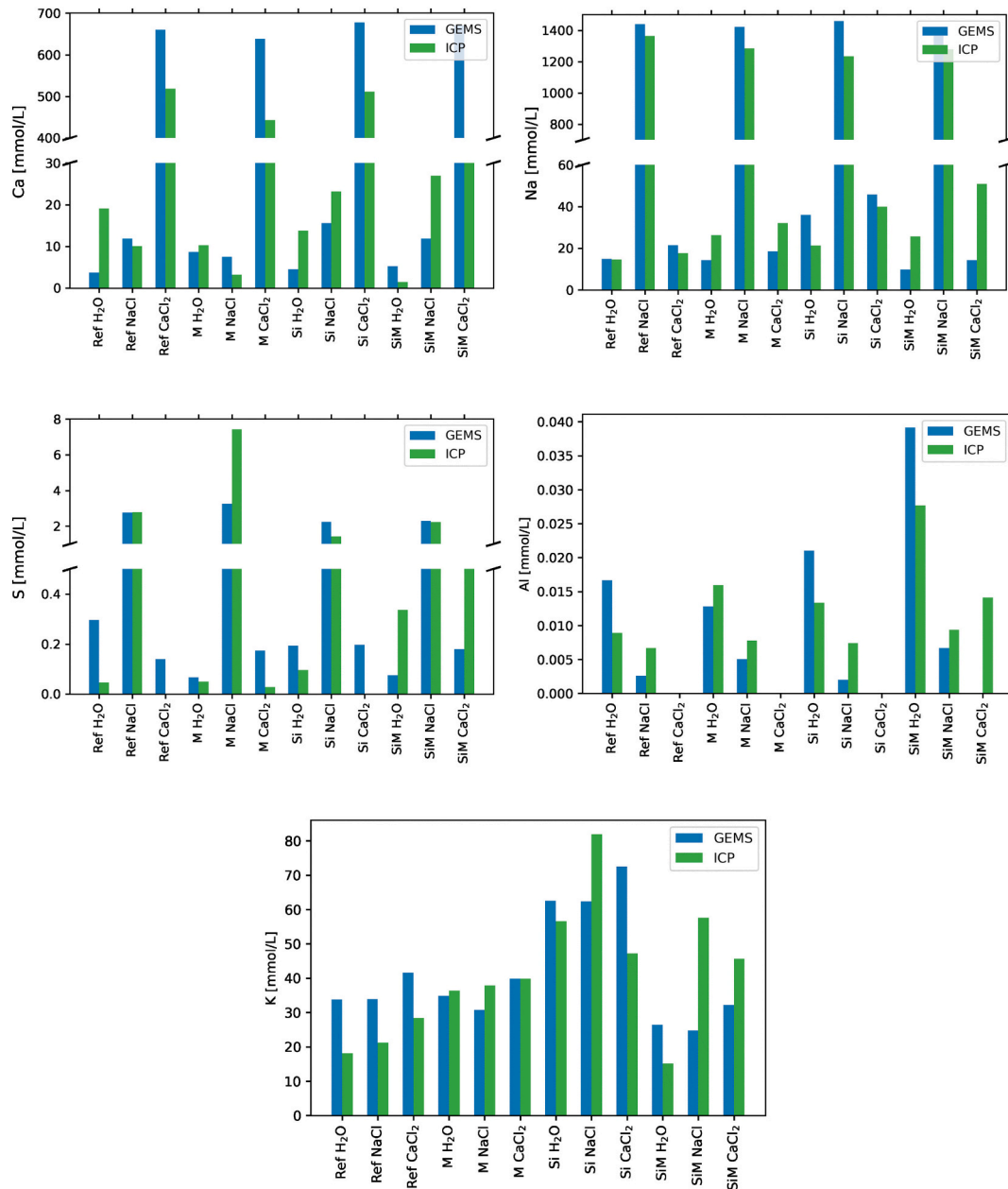
Fig. 12. Calcium, sodium, sulphate, aluminium and potassium concentrations in the exposure solution measured by ICP-AES and predicted by thermodynamic modelling (GEMS) for the Ref, M, Si and SiM binder's pastes exposed to water, NaCl or CaCl$_2$ solutions with a 2 mol/L chloride concentration.

4.2.2. Hydrate assemblage of chloride-exposed samples (NaCl and CaCl$_2$)

4.2.2.1. Chemical chloride binding.
When comparing the predicted phase assemblage for exposure to NaCl and CaCl$_2$ to the phase assemblage for each binder upon exposure to H$_2$O (Fig. 1), the main difference is the transformation of monocarbonate to Friedel's salt. The changes in the quantities of the other phases are rather small. From Fig. 3, minor but systematic variations may be observed in the portlandite content. This depends on the exposure solution, as the portlandite content decreases in the order H$_2$O > NaCl > CaCl$_2$. Fig. 13 shows that the thermodynamic modelling predicts a slight increase in the Friedel's salt content for CaCl$_2$ exposure, compared to NaCl exposure, which is in agreement with [19].

The XRD spectra of the chloride-exposed cement paste samples in Fig. 4 confirm the presence of ettringite and Cl-AFm, independent of the binder type and exposure (NaCl or CaCl$_2$), as predicted by thermodynamic modelling. It should be noted that there are shifts in the position of the Cl-AFm peak in the XRD diffractograms, which could indicate variations in the composition [26,29,55].

The ^{27}Al NMR spectra in Fig. 5 show that the amount of aluminium in AFt decreases slightly for NaCl exposure, compared to the water-exposed samples. However, the AFt content for CaCl$_2$ exposure is similar, or even slightly higher, compared to the water-exposed samples. An indication of a slight increase in ettringite for CaCl$_2$ exposure may also be seen from the DTG curves in Fig. 2, as the peak just above 120 °C seems greater for all the CaCl$_2$-exposed samples when comparing them to the water-exposed and NaCl-exposed ones. However, a potential AFt decrease upon exposure to NaCl compared to water exposure is, not that evident based on the DTG curves. All things considered, the overall changes in the amount of AFt upon exposure to the NaCl or CaCl$_2$ solutions compared to water exposure are rather small. Thus, the AFt in the system will have a similar influence on the chloride binding of the cement pastes for the investigated exposure conditions.

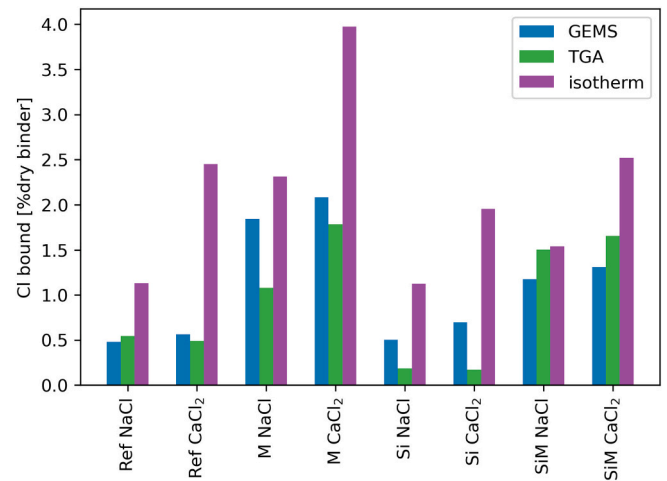The ^{27}Al NMR spectra in Fig. 5 show also that the chloride-exposed
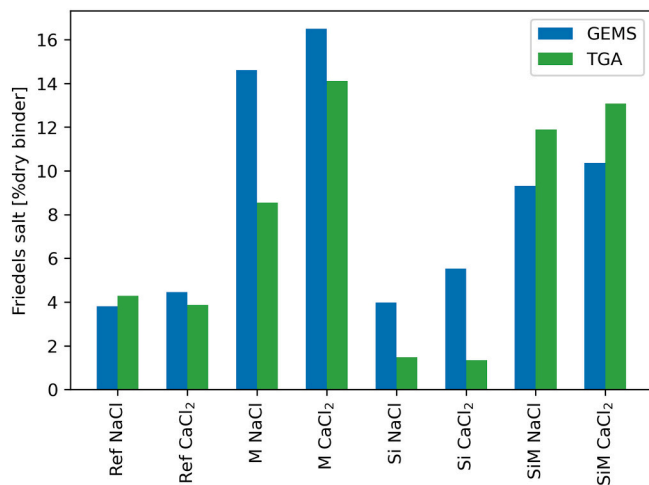
Fig. 13. Comparison of the Friedel's salt content per dry binder predicted by GEMS and the amount of Cl-AFm determined by TGA for pastes with added NaCl or CaCl₂ solution (at a chloride concentration of 2 mol/L).

Fig. 14. Comparison of the amounts of bound chlorides for the NaCl and CaCl₂ exposure (2 mol/L chloride concentration), as predicted by thermodynamic modelling and determined by TGA, based on the Cl-AFm content (assuming the stoichiometry of Friedel's salt and using the chloride-binding isotherms). The total amount of bound chloride obtained from the binding isotherms (Fig. 10) and the chemical binding calculated based on Cl-AFm contents have been normalized to the dry binder mass at 800 °C, using the bound water measured by TGA (Table 4).

samples display larger intensities for aluminium in AFm phases, compared to the water-exposed samples (H₂O), which indicates a greater quantity of AFm phases. There is also a change in the chemical shift corresponding to the AFm phases towards lower ppm's indicating the formation of Cl-AFm [56,57] instead of other AFm phases [58]. The M binder's samples appear to have the greatest amount of AFm phases, followed by SiM, Ref and finally Si binders, as anticipated from the Al content of these systems (Table 1). However, based on the ^{27}Al NMR spectra, the amount of AFm has no clear dependency on the cation (NaCl vs. CaCl₂).

The DTG curves allow the Cl-AFm content in the pastes to be quantified. The main difference in the DTG curves for the chloride-exposed pastes, compared to the curves for the water-exposed samples shown in Fig. 2, is the appearance of a pronounced mass-loss peak between 300 and 400 °C. This peak relates to the decomposition of Cl-AFm [32]. The mass loss was determined by integrating the DTG curve in the temperature interval of Cl-AFm, and the respective amount of Cl-AFm was calculated according to [23,34], as described in Section 3.3.3. The predicted amount of Cl-AFm and measured amount using TGA are compared in Fig. 13. The measured Cl-AFm content in the samples of Ref and Si binder seems somewhat independent of the cation in the exposure solution (NaCl vs. CaCl₂). For the samples of M and SiM binder's pastes, the Cl-AFm content seems slightly higher for the CaCl₂ exposure compared to NaCl exposure. While this applies only to the SiM binder for the ^{27}Al NMR results in this study, these findings are in line with the thermodynamic predictions and could be related to the lower pH in the CaCl₂ systems compared to the NaCl systems. This would lead to a higher Ca concentration in the solution, and lower Al uptake in the C (-A)-S-H (Fig. 7), which favours a higher AFm content. Also, the M and SiM binders both contain metakaolin, which is known to be a very reactive aluminium-containing pozzolan. The result is a composite cement with a relatively low Ca/(Al + Si) ratio. The additional calcium provided by exposure to CaCl₂ may have enabled the formation of additional Cl-AFm, as described previously by [15,19,24].

In Fig. 14, the total amount of bound chloride from the binding isotherms at 2 mol/L chloride for both NaCl and CaCl₂ exposure is compared to the amount of chemically bound chlorides. This is calculated based on the Cl-AFm content determined using TGA as well as the amounts predicted by thermodynamic modelling. The following ideal stoichiometry has been assumed for Friedel's salt: C₃A.CaCl₂.10H₂O for the calculations. The total amount of bound chloride obtained from the binding isotherms (Fig. 10) and the chemical binding calculated based on Cl-AFm contents have been normalized to the dry binder mass at

800 °C, using the bound water measured by TGA (Table 4).

It should be noted that the above-mentioned stoichiometry for Friedel's salt (Cl/Al molar ratio = 1) represents the composition of Cl-AFm containing the highest possible content of chlorides. The AFm phases can accommodate various anions such as carbonate, sulfate, hydroxyl and chloride ions [27,59]. Friedel's salt is the end member with the highest chloride content. Hemstad et al. [29] showed recently that, among other things, the chloride content in AFm can vary depending in the pH of the exposure solution. At a pH of 13, they measured a Cl/Al molar ratio of the AFm of only 0.5, meaning 50 % of the ideal stoichiometry of Friedel's salt. However, at a pH of 12 or lower the Cl/Al ratio approached 1. In the present work, the authors have not determined the exact composition of Cl-AFm for each of the binders and exposure conditions. Hence, it is not possible to conclude on the exact contribution of Cl-AFm to the total amounts of bound chlorides in the paste. Thus, when presenting the bound chlorides based on the TGA results in Fig. 14, this merely indicates a maximum potential contribution of Cl-AFm to the total level of bound chlorides.

The amount of bound chlorides determined from the binding isotherm are generally much higher (more than double for Ref, M, Si binders) than the amount predicted by thermodynamic modelling, and the amount of chlorides assumed to be found in Friedel's salt, except for the sample of SiM binder exposed to NaCl (SiM NaCl). The underestimation of bound chlorides by the thermodynamic model compared to the isotherm is due to physical chloride binding by the C(-A)-S-H which is not considered in the model. The model only accounts for the chloride bound in the AFm which is also the case for the TGA determination and therefore these two agree rather well.

4.2.2.2. Physical chloride binding. In Fig. 15, the calculated amount of physically bound chlorides at 2 mol/L chloride for both NaCl and CaCl₂ exposure is compared with the predicted amount of physically bound chloride estimated based on the relation presented by Georget et al. [60] which correlates the Cl/Si ratio of C(-A)-S-H to the concentration of calcium in the exposure solution. The amount of physically bound chloride was calculated subtracting the chemically bound chloride in Cl-AFm, determined using either TGA or thermodynamic modelling (Fig. 14), from the total amount of bound chlorides read from the binding isotherms. The total amount of bound chloride obtained from
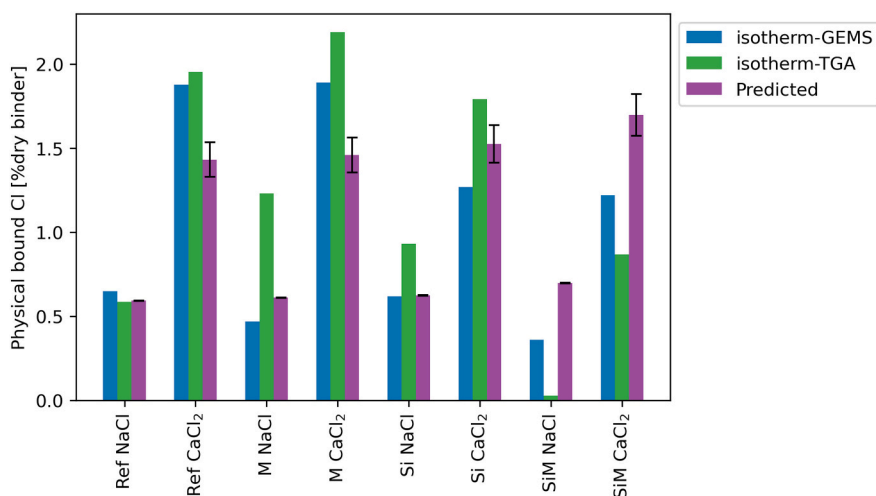
Fig. 15. Comparison of the calculated amount of physically bound chlorides for the NaCl and CaCl₂ exposure (2 mol/L chloride concentration), with the upper and lower level of the predicted amount of physically bound chloride estimated based on the relation presented by Georget et al. [60]. The calculated bound chlorides were accounted for by subtracting the chemically bound chloride content (based on the Cl-AFm content determined using TGA and GEMS) from the total amount of bound chlorides from the binding isotherms at 2 mol/L chloride for both NaCl and CaCl₂ exposure. The total amount of bound chloride obtained from the binding isotherms (Fig. 10) and the chemical binding calculated based on Cl-AFm contents have been normalized to the dry binder mass at 800 °C, using the bound water measured by TGA (Table 4).

the binding isotherms (Fig. 10) and the chemical binding calculated based on Cl-AFm contents have been normalized to the dry binder mass at 800 °C, using the bound water measured by TGA (Table 4).

For the calculation of chemically bound chlorides based on the Cl-AFm content determined using TGA, the following ideal stoichiometry for Friedel's salt was assumed: $C_3A.CaCl_2.10H_2O$. The estimation of the predicted physically bound chlorides was performed according to Eq. (5) [60]:

$$Cl_{C(-A)-S-H} = \left[(0.132 \pm 0.016) \times [Ca^{2+}] + 0.059 \right] \times Si_{C(-A)-S-H} \quad (5)$$

The values for $[Ca^{2+}]$ and $Si_{C(-A)-S-H}$ were predicted by thermodynamic modelling (GEMS). The calculation sheets of predicted physically bound chlorides are provided as appended data.

The calculated and predicted amounts of physically bound chlorides seem to have an acceptable agreement, especially for the Ref binder, considering the uncertainties behind prediction of each of these values. The results infer a pronounced sensitivity to the associated cation, in NaCl vs CaCl₂, and an increase in physical binding in the case of CaCl₂ exposure compared to NaCl exposure. This can be due to the higher concentration of calcium in the exposure solution when binders are exposed to CaCl₂ [4,19]. The calculated physically bound chloride amounts show a clear variation upon changes in binder composition. The predicted physically bound chloride amounts according to Georget et al. [60], seem not to take up on the variations in physical binding due to the different binder compositions. This is due to the lack of changes in $Si_{C(-A)-S-H}$, as a consequence of the implementation of C(-A)-S-H solid solutions in the presence of portlandite in thermodynamic modelling.

Aside from the effect of concentration of calcium on physical binding of chlorides, it is reported that aluminium substitution in C(-A)-S-H decreases the adsorption sites and, consequently the chloride-binding potential [61]. Therefore, the lowered Al/Si molar ratio of the C(-A)-S-H enhances the physical binding of chlorides. Moreover, exposure to chloride solutions affects the C(-A)-S-H chain length which, as reported by Yoshida et al. [61], affects the chemical composition of C(-A)-S-H and, consequently, the adsorption sites and potential for chloride adsorption. The increased amounts of bound chlorides may also be related to the increase in Ca²⁺ ions accumulated in the Stern layer of the C(-A)-S-H [17,62]. In short, several processes, i.e. chain length, adsorption sites, total surface area of C(-A)-S-H and concentration of calcium ions, play a role when accounting for the physically bound chloride content.

To illustrate the impact of chloride exposure on the C(-A)-S-H composition of the different investigated binders, the ²⁹Si NMR spectra shown in Fig. 6 are replotted for each binder in Fig. 16 presented in Appendix A. The most remarkable change in the ²⁹Si NMR spectra

upon chloride exposure (NaCl and CaCl₂) compared to water exposure is the reduction in the Q² (Al) peak. This relates to the amount of bridging silicon tetrahedral sites containing an Al atom instead of a Si atom. This is most prominent for the metakaolin-containing samples (from M and SiM binder's pastes), which have the most pronounced Q² (Al) peaks for water exposure. Upon chloride exposure, the Q¹ and Q² peaks in the ²⁹Si NMR spectra seem to increase at the expense of the Q² (Al) peak (see Figs. 6 and 14). The reduction in the amount of alumina as bridging tetrahedra in the C(-A)-S-H is also confirmed by the ²⁷Al NMR spectra shown in Fig. 9. This shows that the signal for the four-fold coordinated bridging alumina is considerably lower for the chloride-exposed pastes (NaCl and CaCl₂) compared to the water-exposed ones, with CaCl₂-exposed samples having the lowest signal. It may be concluded that the presence of chloride reduces the uptake of aluminium in C(-A)-S-H with the impact strongest for CaCl₂ exposure, as shown in Fig. 8. When compared to the ranges reported in the literature ca. 0.001–0.2 [63], the scale of observed changes in the aluminium uptake of C(-A)-S-H induced by exposure of the system to chloride ions seems considerable. A hypothesis for the effect of chloride exposure on the Al-content of the C-(A)-S-H might be that Cl-AFm has greater stability compared to C(-A)-S-H. This would be a reasonable assumption as long as the solubility of C(-A)-S-H is closer to C-S-H (log K_{S0} = −6 to −11 [64] for [41]) than Cl-AFM (log K_{S0} = −27.27 [41]). This results in the formation of additional chloride-containing AFm phases, instead of Al-uptake in C(-A)-S-H. For CaCl₂ exposure, more Cl-AFm may be formed and thereby the Al-uptake in C(-A)-S-H is lowered further. Therefore, chloride exposure affects also the calculated chain length (CL) of the C(-A)-S-H, as shown in Fig. 7. NaCl exposure leads to an increase in the calculated chain length, whereas CaCl₂ exposure leads to a similar or even slightly reduced chain length compared to the water-exposed pastes.

4.2.2.2.1. Summary of changes in hydrate assemblage for the different binders upon chloride exposure. In Table 5, a comparison of the main investigated characteristics of the hydrate assemblage for the four binders exposed to water, NaCl and CaCl₂ solution were presented. Table 6 summarizes the general trends observed of the impact of the exposure solution (CaCl₂ vs NaCl, NaCl vs Water and CaCl₂ vs water) on pH and [Ca²⁺] concentration of the exposure solution (Fig. 12); modelled amount of AFm, AFt and C(-A)-S-H formed (Fig. 1); calculated chain length (CL) and Al/Si ratio of the C(-A)-S-H and measured total bound chloride (Fig. 10) for all investigated binders.

The presented trends in Table 6, infer that the associated cation in exposure chloride solutions play a key role in accounting for chloride binding among other parameters, such as chain length, Al/Si ratio and concentration of calcium ions. This further emphasizes the importance of considering both NaCl and CaCl₂ exposure solutions when studying chloride binding phenomenon.

Table 6

Summary of general trends observed of the impact of the exposure solution (CaCl$_2$ vs NaCl, NaCl vs Water and CaCl$_2$ vs water) on: pH and [Ca2+] concentration of the exposure solution; modelled amount of Cl-AFm, AFt and C(-A)-S-H formed; calculated chain length (CL) and Al/Si ratio of the C(-A)-S-H and total measured bound chloride for all investigated binders.

	pH	[Ca^{2+}] mmol/L	AFm [g/100 g binder]	AFt [g/100 g binder]	C(-A)-S-H [g/100 g binder]	C(-A)-S-H (CL)	C(-A)-S-H Al/Si	Total bound chloride
CaCl$_2$ vs NaCl	↓	↑	↑	–[a]	–	↓	↓	↑
NaCl vs water	–	↓ for Ref&M binders ↑for Si&SiM binders	↑	–	–	↑	↓	Not relevant
CaCl$_2$ vs water	↓	↑	↑	–	–	↓	↓	Not relevant

[a] The horizontal line indicates no change.

For all binders, the total amount of bound chlorides from the binding isotherm increases for exposure to CaCl$_2$ compared to NaCl, whereas the Cl-AFm content is only slightly increased. This is in line with previous studies [4,19,29,30,50], in which the difference between the total amount of bound chlorides and the chloride bound in AFm was ascribed to physical binding in the C(-A)-S-H. For CaCl$_2$, the physical binding in the C(-A)-S-H increases due to the decrease in pH and increase in solution's Ca^{2+} concentration. This causes an accumulation of Ca^{2+} in the Stern layer [62], resulting in an apparent reversal of the originally negative surface charge of the C(-A)-S-H [62] and consequently a higher accumulation of the negatively charged chloride ions in the diffuse layer of the C(-A)-S-H [17,18]. This effect should be valid for all binders for which the pore solution is buffered by portlandite or possibly high Ca/Si ratio C(-A)-S-H phases of the Jennite type [61,65]. Only for very low Ca/Si ratios such as tobermorite-like structures will the chloride binding of C(-A)-S-H phases be low [61,66]. Chloride exposure leads to a reduction in the Al/Si molar ratio of the C(-A)-S-H and a higher chain length (CL) upon exposure to NaCl. For exposure to CaCl$_2$ the effect on reduction of Al/Si molar ratio of the C(-A)-S-H is stronger compared to NaCl, while the chain length of the C(-A)-S-H decreases instead. This results in an increase in the predicted amount of AFm formed upon chloride exposure, which is also confirmed by the experimental results.

4.3. Can the changes in the phase assemblage explain the differences in observed binding behaviour?

Table 7 summarizes general trends observed of the impact of the binder composition (SCM containing binders vs Ref) on pH and [Ca^{2+}] concentration of the exposure solution (Fig. 12); amount of measured Cl-AFm (Fig. 13), modelled AFt and C(-A)-S-H formed (Table 5); calculated chain length (CL) (Table 5) and Al/Si ratio of the C(-A)-S-H (Table 5) and total measured bound chloride (Fig. 10) for all investigated binders. The black arrows represent exposure to NaCl solution and green arrows stand for exposure to CaCl$_2$ solution.

For the silica fume-containing paste (Si), the total amount of bound chloride is rather similar (exposure to NaCl) or slightly decreased (exposure to CaCl$_2$) compared to the one for the Portland reference (Ref). However, the amount of Cl-AFm is considerably lower (see Fig. 13). The reason why the Ref and Si binder's samples have a similar total amount of bound chlorides can be explained by several phenomena acting simultaneously. First, the chloride content in the Cl-AFm formed in the Ref binder's sample is not necessarily similar to that in the Si sample. Hemstad et al. [29] showed that the chloride content in Cl-AFm increases with decreasing pH. In this study, the exposure solution for Si paste has a lower pH at equilibrium compared to the Ref binder's sample (see Fig. 11). This can result in a higher chloride content in the Cl-AFm in the Si sample compared the one in the Ref binder's sample. Second, the difference between the total bound chloride content and the chlorides in the Cl-AFm can be attributed to physical binding in the C(-A)-S-H. As the pH of the exposure solution of the Si binder's samples is lower than the pH in the Ref binder's sample, the C(-A)-S-H in the Si sample might be able to physically bind more chlorides [21]. Furthermore, the Si sample simply has a higher C(-A)-S-H content compared to the Ref binder's sample, with a lower Al/Si ratio, thereby contributing to a

higher degree of physical binding.

The metakaolin-containing paste (M) can bind the highest quantity of chlorides of all tested binders (Fig. 13). The M binder's samples have a considerably higher Cl-AFm content compared to the samples of Ref and Si binder. The total amount of bound chlorides and the Cl-AFm content is higher for CaCl$_2$ exposure than for NaCl exposure. Thus, for the M binder's paste, the increase in chloride binding when comparing CaCl$_2$ with NaCl exposure cannot be attributed solely to increased physical binding in the C(-A)-S-H, as first put forward in [4]. This is because an increase in the amount of Cl-AFm was also observed, as reported by [19,23]. The results reported from this work suggest that in the case of exposure to CaCl$_2$ compared to NaCl, the amount of Cl-AFm increases in M binder, while the uptake of aluminium in the C(-A)-S-H is decreased. As mentioned before, the authors cannot draw precise conclusions as to the contribution of Cl-AFm to the total level of bound chlorides. However, we can attribute part of the increase in the total amounts of bound chlorides in the M binder's samples (compared to the reference sample) to an increase in the amount of Cl-AFm. The uptake of chlorides in the C(-A)-S-H although might be positively affected by the higher quantity of C(-A)-S-H in the system but is also negatively affected by the more polymerised C(-A)-S-H and its higher aluminium uptake as well as the lower concentration of calcium in the exposure solution.

In the SiM binder's paste, when metakaolin is combined with silica fume as a replacement for the Portland cement, the result is a slightly increased (exposure to NaCl) or similar total amount of bound chlorides (exposure to CaCl$_2$), compared to the reference Portland paste (Fig. 10). Silica fume seems to counter act the enhancing effect of metakaolin on chloride binding. ^{29}Si NMR data in Figs. 6 and 16 suggests that both, silica fume and metakaolin, have reacted as neither Q^3 or Q^4 intensities were observed and all portlandite is consumed. Hence a competition of silica fume and metakaolin hydration is unlikely the explanation for this result. To explain this, the chloride-binding phases need to be examined. The Cl-AFm content determined by TGA in the samples of SiM binder is almost similar to the content in the samples of M binder (Fig. 13). However, this does not necessarily mean that the level of chlorides bound in the AFm is the same for both cases. This is because the chloride content of the AFm may vary depending on the pH [29]. Nevertheless, the SiM binder's paste has a slightly lower pH compared to the M binder's paste (Fig. 11) and would, therefore, lead to the higher Cl uptake by the Cl-AFm, as observed by Hemstad et al. [29]. Thus, the lower total amounts of bound chlorides in the SiM binder's samples compared to the M binder's samples, is likely to be related largely to changes in the physical binding of the C(-A)-S-H. The C(-A)-S-H of the SiM binder's samples has the longest chain length and highest Al/Si ratio of all investigated binders. In addition, the SiM binder's samples have the lowest pH at equilibrium and are portlandite-deficient. The latter might cause lower calcium and hydroxyl concentrations in the pore solution and, thereby, reduce the physical binding in the C(-A)-S-H [21,22]. Further research is needed to confirm and quantify this aspect.

5. Conclusion

Hydrated cement pastes were prepared using the following four binders: plain Portland cement (PC), PC with 15 wt% silica fume

Table 7
Summary of general trends observed of the impact of the binder composition (SCM containing binders *vs* Ref) on: pH and [Ca²⁺] concentration of the exposure solution; amount of measured Cl-AFm, modelled AFt and C(-A)-S-H formed; calculated chain length (CL) and Al/Si ratio of the C(-A)-S-H and measured total bound chloride for all investigated binders. The black arrows represent exposure to NaCl solution and green arrows stand for exposure to CaCl₂ solution.

Binder system	pH		[Ca²⁺] mmol/L				AFm [g/100 g binder]		AFt [g/100 g binder]		C(-A)-S-H [g/100 g binder]		C(-A)-S-H (CL) [–]		C(-A)-S-H Al/Si [–]		Total bound chloride	
	NaCl	CaCl₂	NaCl-modelled	CaCl₂-modelled	NaCl-measured	CaCl₂-measured	NaCl	CaCl₂	NaCl	CaCl₂	NaCl	CaCl₂	NaCl	CaCl₂	NaCl	CaCl₂	NaCl	CaCl₂
Si	–ᵃ	→	→	→	→	→	→	→	–	–	→	→	→	→	→	→	–	→
M	–	→	→	→	→	→	→	←	–	–	←	←	←	–	←	←	←	←
SiM	–	→	–	→	←	→	←	←	–	–	←	←	←	←	←	←	←	–

ᵃ The horizontal line indicates no change.

replacement, PC with 15 wt% metakaolin replacement and PC with 15 wt% metakaolin and 15 wt% silica fume replacement (total 30 wt%). The crushed hydrated cement pastes were exposed to water, NaCl or CaCl₂ solutions and left to equilibrate. After equilibration, the chloride-binding isotherms were determined and the exposure solution was characterized in terms of its pH and elemental composition. The hydrate assemblage was investigated for the water and NaCl and CaCl₂ solutions, both with 2 mol/L chloride concentration, using TGA, XRD, ²⁷Al NMR and ²⁹Si NMR. The experimental findings were compared to thermodynamic calculations of the phase assemblages of these binder systems.

Comparison of the ²⁷Al NMR and ²⁹Si NMR results of the chloride-exposed samples with the water-exposed samples showed that chloride exposure reduces the aluminium uptake in the C(-A)-S-H. This results in an increased amount of Cl-AFm formed. The reduction in aluminium uptake is stronger for CaCl₂ exposure compared to NaCl exposure. This is partly the reason for the observed higher chloride binding in CaCl₂ exposed binders compared to NaCl.

The amount of Cl-AFm was determined based on DTG curves. Even accounting for pure Friedel's salt, it is not possible to explain the total amounts of bound chlorides from isotherms solely by the binding in Cl-AFm. Thus, physical binding by the most abundant hydrate, C(-A)-S-H, plays an important role in the actual binding of the investigated cement pastes.

The estimated bound chloride quantities indicated that higher amounts of binding of chloride can be expected upon exposure to CaCl₂ compared to NaCl. The explanation for this well-known observation based on the obtained results in this study is concluded to be twofold. The increased amount of Cl-AFm formed, due to the higher reduction in aluminium uptake in the C(-A)-S-H when binders are exposed to CaCl₂ is one explanation. Further, the estimated physically bound chloride quantities indicated that higher amounts of physical binding of chloride can be expected upon exposure to CaCl₂ compared to NaCl. This was explained by the higher concentration of calcium in the exposure solution as well as the lower aluminium uptake and Al/Si ratio of the C(-A)-S-H. The results indicated that the difference in physically bound chloride amounts due to changes in the composition of binder systems had a less pronounced effect than in the case of changing the accompanying ion in chloride solution.

The impact of the binder composition may be summarised as follows:

- Increasing the amount of silicates in the system, by replacing 15 % of the PC with silica fume, did not change the amounts of bound chlorides compared to the PC reference, even though a slightly lower amount of Cl-AFm was measured. This indicates that either the chloride content in the Cl-AFm increased and/or that the physical binding in the C(-A)-S-H increased. A higher quantity of physical binding might be attributed to the higher content of C(-A)-S-H in the system and the reduction in its aluminium uptake.
- Increasing the amount of alumina and silicate in the system, by replacing 15 % of the PC with metakaolin, resulted in an increased amount of bound chlorides compared to the PC reference. This increase was mainly attributed both to more Cl-AFm in the system. The uptake of chlorides in the C(-A)-S-H although might be positively affected by the higher quantity of C(-A)-S-H in the system but are also negatively affected by the more polymerised C(-A)-S-H and its higher aluminium uptake, as well as the lower concentration of calcium in the exposure solution.
- Replacing the PC with a combination of 15 % metakaolin and 15 % silica fume, resulted in a portlandite deficient system, which had a similar or only slightly higher total amount of bound chlorides compared to the PC reference. Thus, the combined metakaolin and silica-fume system has a lower chloride-binding capacity compared to the system containing only metakaolin. This, despite SiM system has higher cl-AFm content compared to PC, thereby, indicates that the relative reduction in chloride binding is largely due to a

reduction in physical binding by the more polymerised C(-A)-S-H and its higher aluminium uptake.

CRediT authorship contribution statement

Arezou Babaahmadi: conceptualization, methodology, software, formal analysis, investigation, writing – original draft, review & editing, supervision, funding acquisition, project administration.

Alisa Machner: conceptualization, methodology, writing – original draft, software, review & editing, validation, supervision.

Wolfgang Kunther: conceptualization, methodology, writing – review & editing, software, validation, supervision.

João Figueira: Investigation.

Petter Hemstad: methodology, software.

Klaartje De Weerdt: conceptualization, methodology, software, formal analysis, writing – original draft, review & editing, visualization, validation, supervision.

Declaration of competing interest

The authors declare that they have no known competing financial interests or personal relationships that could have appeared to influence the work reported in this paper.

Appendix A

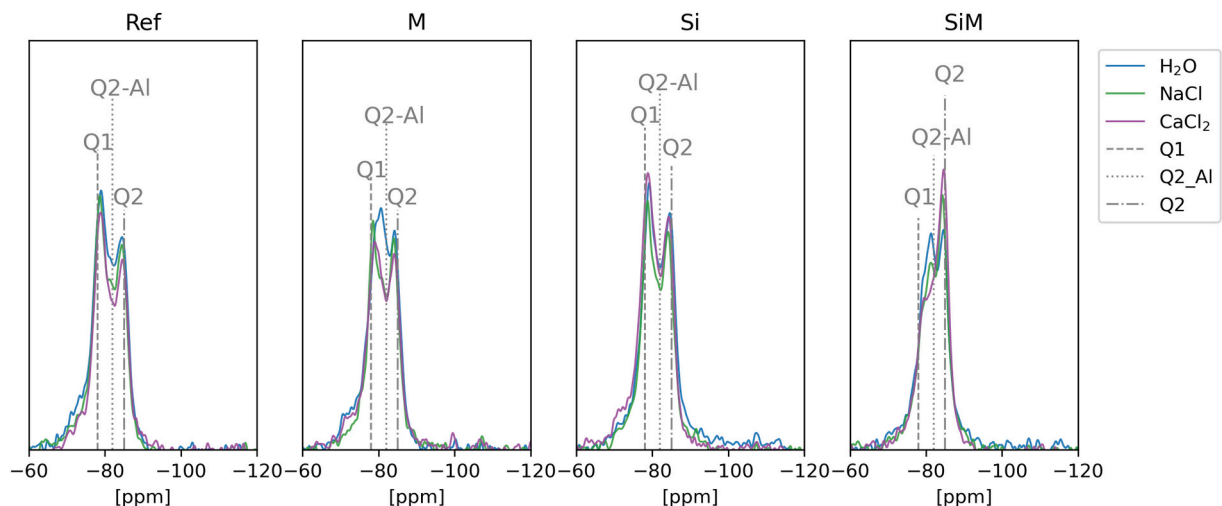**Fig. 16.** Normalized ^{29}Si NMR spectra for the Ref, M, Si and SiM cement pastes exposed to water (H_2O), NaCl or $CaCl_2$ solution. The Q1 (silicon end-members tetrahedron), Q2_Al (bridging tetrahedron connected to Al) and Q2 (bridging tetrahedron) are indicated by lines in the figures as a visual guide. This is the same data as for Fig. 6 but organised by binder instead of exposure.

Appendix B. Supplementary data

Supplementary data to this article can be found online at https://doi.org/10.1016/j.cemconres.2022.106924.

References

[1] E. Gartner, Industrially interesting approaches to "low-CO2" cements, Cem. Concr. Res. 34 (2004) 1489–1498.
[2] G. Schmitt, Global Needs for Knowledge Dissemination, Research, And Development in Materials Deterioration And Corrosion Control, World Corrosion Organization, New York, 2009.
[3] M.G. Stewart, X. Wang, M.N. Nguyen, Climate change adaptation for corrosion control of concrete infrastructure, Struct. Saf. 35 (2012) 29–39.
[4] K. De Weerdt, A. Colombo, L. Coppola, H. Justnes, M.R. Geiker, Impact of the associated cation on chloride binding of Portland cement paste, Cem. Concr. Res. 68 (2015) 196–202.
[5] M. Balonis, B. Lothenbach, G. Le Saout, F.P. Glasser, Impact of chloride on the mineralogy of hydrated Portland cement systems, Cem. Concr. Res. 40 (2010) 1009–1022.
[6] K. De Weerdt, D. Orsáková, M.R. Geiker, The impact of sulphate and magnesium on chloride binding in Portland cement paste, Cem. Concr. Res. 65 (2014) 30–40.
[7] K. De Weerdt, D. Orsáková, A.C.A. Müller, C.K. Larsen, B. Pedersen, M.R. Geiker, Towards the understanding of chloride profiles in marine exposed concrete, impact of leaching and moisture content, Constr. Build. Mater. 120 (2016) 418–431.
[8] R. Dhir, M. El-Mohr, T. Dyer, Chloride binding in GGBS concrete, Cem. Concr. Res. 26 (1996) 1767–1773.
[9] M. Florea, H. Brouwers, Chloride binding related to hydration products: part I: ordinary Portland cement, Cem. Concr. Res. 42 (2012) 282–290.
[10] H. Justnes, A review of chloride binding in cementitious systems, in: Nordic Concrete Research-Publications- 21, 1998, pp. 48–63.
[11] M. Sharfuddin Ahmed, O. Kayali, W. Anderson, Chloride penetration in binary and ternary blended cement concretes as measured by two different rapid methods, Cem. Concr. Compos. 30 (2008) 576–582.
[12] L. Tang, L.-O. Nilsson, Chloride binding capacity and binding isotherms of OPC pastes and mortars, Cem. Concr. Res. 23 (1993) 247–253.
[13] Q. Yuan, C. Shi, G. De Schutter, K. Audenaert, D. Deng, Chloride binding of cement-based materials subjected to external chloride environment – a review, Constr. Build. Mater. 23 (2009) 1–13.
[14] H. Zibara, Binding of External Chlorides by Cement Pastes [microform], University of Toronto, 2001.
[15] H. Zibara, R.D. Hooton, M.D.A. Thomas, K. Stanish, Influence of the C/S and C/A ratios of hydration products on the chloride ion binding capacity of lime-SF and lime-MK mixtures, Cem. Concr. Res. 38 (2008) 422–426.
[16] J.J. Beaudoin, V.S. Ramachandran, R.F. Feldman, Interaction of chloride and C S H, Cem. Concr. Res. 20 (1990) 875–883.

[17] G. Plusquellec, A. Nonat, Interactions between calcium silicate hydrate (C-S-H) and calcium chloride, bromide and nitrate, Cem. Concr. Res. 90 (2016) 89–96.

[18] O. Wowra, M.J. Setzer, Sorption of chlorides on hydrated cements and C3A pastes, in: Frost Resistance of Concrete, E& FN Spon, 1997.

[19] Z. Shi, M.R. Geiker, K. De Weerdt, T.A. Østnor, B. Lothenbach, F. Winnefeld, J. Skibsted, Role of calcium on chloride binding in hydrated Portland cement–metakaolin–limestone blends, Cem. Concr. Res. 95 (2017) 205–216.

[20] Q. Zhu, L. Jiang, Y. Chen, J. Xu, L. Mo, Effect of chloride salt type on chloride binding behavior of concrete, Constr. Build. Mater. 37 (2012) 512–517.

[21] J. Tritthart, Chloride binding in cement II.The influence of the hydroxide concentration in the pore solution of hardened cement paste on chloride binding, Cem. Concr. Res. 19 (1989) 683–691.

[22] Y. Zhou, D. Hou, J. Jiang, L. Liu, W. She, J. Yu, Experimental and molecular dynamics studies on the transport and adsorption of chloride ions in the nano-pores of calcium silicate phase: the influence of calcium to silicate ratios, Microporous Mesoporous Mater. 255 (2018) 23–35.

[23] Z. Shi, M.R. Geiker, B. Lothenbach, K. De Weerdt, S.F. Garzón, K. Enemark-Rasmussen, J. Skibsted, Friedel's salt profiles from thermogravimetric analysis and thermodynamic modelling of Portland cement-based mortars exposed to sodium chloride solution, Cem. Concr. Compos. 78 (2017) 73–83.

[24] M. Thomas, R. Hooton, A. Scott, H. Zibara, The effect of supplementary cementitious materials on chloride binding in hardened cement paste, Cem. Concr. Res. 42 (2012) 1–7.

[25] H. Maraghechi, F. Avet, H. Wong, H. Kamyab, K. Scrivener, Performance of Limestone Calcined Clay Cement (LC3) with various kaolinite contents with respect to chloride transport, Mater. Struct. 51 (2018) 125.

[26] F. Avet, K. Scrivener, Influence of pH on the chloride binding capacity of Limestone Calcined Clay Cements (LC3), Cem. Concr. Res. 131 (2020), 106031.

[27] M. Balonis, The Influence of Inorganic Chemical Accelerators And Corrosion Inhibitors on the Mineralogy of Hydrated Portland Cement Systems, University of Aberdeen Aberdeen, UK, 2010.

[28] A. Machner, P. Hemstad, K. De Weerdt, Towards the understanding of the pH dependency of the chloride binding of Portland cement pastes, Nord.Concr.Res. 58 (2018) 143–162.

[29] P. Hemstad, A. Machner, K. De Weerdt, The effect of artificial leaching with HCl on chloride binding in ordinary Portland cement paste, Cem. Concr. Res. 130 (2020), 105976.

[30] A. Machner, M. Zajac, M.Ben Haha, K.O. Kjellsen, M.R. Geiker, K.De Weerdt, Stability of the hydrate phase assemblage in Portland composite cements containing dolomite and metakaolin after leaching, carbonation, and chloride exposure, Cem. Concr. Compos. 89 (2018) 89–106.

[31] B. Traynor, H. Uvegi, E. Olivetti, B. Lothenbach, R.J. Myers, Methodology for pH measurement in high alkali cementitious systems, Cem. Concr. Res. 135 (2020), 106112.

[32] B. Lothenbach, P. Durdzinski, K. De Weerdt, Thermogravimetric analysis - chapter 5, in: K. Scrivener, R. Snellings, B. Lothenbach (Eds.), A Practical Guide to Microstructural Analysis of Cementitious Materials, 1st ed., CRC Press, 2016.

[33] T. Otake, S. Tone, I. Komasawa, M. Kawashima, Involvement of solid acids in the thermal decomposition of calcium chloride, Kagaku Kogaku Ronbunshu 9 (1983) 523–529.

[34] C. Qiao, P. Suraneni, N. Then, A. Choudhary, W. Weiss, Chloride binding of cement pastes with fly ash exposed to CaCl2 solutions at 5 and 23 C, 2018.

[35] K. De Weerdt, M.B. Haha, G. Le Saout, K.O. Kjellsen, H. Justnes, B. Lothenbach, Hydration mechanisms of ternary Portland cements containing limestone powder and fly ash, Cem. Concr. Res. 41 (2011) 279–291.

[36] B.M. Fung, A.K. Khitrin, K. Ermolaev, An improved broadband decoupling sequence for liquid crystals and solids, J. Magn. Reson. 142 (2000) 97–101 (San Diego, Calif.: 1997).

[37] I.G. Richardson, A.R. Brough, G.W. Groves, C.M. Dobson, The characterization of hardened alkali-activated blast-furnace slag pastes and the nature of the calcium silicate hydrate (C-S-H) phase, Cem. Concr. Res. 24 (1994) 813–829.

[38] I.G. Richardson, G.W. Groves, The structure of the calcium silicate hydrate phases present in hardened pastes of white Portland cement/blast-furnace slag blends, J. Mater. Sci. 32 (1997) 4793–4802.

[39] D. Kulik, T. Wagner, S. Dmytrieva, G. Kosakowski, F. Hingerl, K. Chudnenko, U. Berner, GEM-selektor geochemical modeling package: revised algorithm and GEMS3K numerical kernel for coupled simulation codes, Comput. Geosci. 17 (2013) 1–24.

[40] T. Wagner, D.A. Kulik, F.F. Hingerl, S.V. Dmytrievava, Gem-selektor geochemical modeling package: TSolMod library and data interface for multicomponent phase models, Can. Mineral. 50 (2012) 1173–1195.

[41] B. Lothenbach, D.A. Kulik, T. Matschei, M. Balonis, L. Baquerizo, B. Dilnesa, G. D. Miron, R.J. Myers, Cemdata18: a chemical thermodynamic database for hydrated Portland cements and alkali-activated materials, Cem. Concr. Res. 115 (2019) 472–506.

[42] J. Skibsted, R. Snellings, Reactivity of supplementary cementitious materials (SCMs) in cement blends, Cem. Concr. Res. 124 (2019), 105799.

[43] A.C.A. Muller, K.L. Scrivener, J. Skibsted, A.M. Gajewicz, P.J. McDonald, Influence of silica fume on the microstructure of cement pastes: new insights from 1H NMR relaxometry, Cem. Concr. Res. 74 (2015) 116–125.

[44] Z. Dai, T.T. Tran, J. Skibsted, Aluminum incorporation in the C-S-H phase of white Portland cement-metakaolin blends studied by 27Al and 29Si MAS NMR spectroscopy, J. Am. Ceram. Soc. 97 (2014) 2662–2671.

[45] A. Machner, M. Zajac, M.Ben Haha, K.O. Kjellsen, M.R. Geiker, K.De Weerdt, Portland metakaolin cement containing dolomite or limestone – similarities and differences in phase assemblage and compressive strength, Constr. Build. Mater. 157 (2017) 214–225.

[46] T. Matschei, B. Lothenbach, F.P. Glasser, The AFm phase in Portland cement, Cem. Concr. Res. 37 (2007) 118–130.

[47] H.J. Kuzel, H. Pöllmann, Hydration of C3A in the presence of Ca(OH)2, CaSO4·2H2O and CaCO3, Cem. Concr. Res. 21 (1991) 885–895.

[48] D. Damidot, S. Stronach, A. Kindness, M. Atkins, F.P. Glasser, Thermodynamic investigation of the CaO Al2O3 CaCO3 H2O closed system at 25°C and the influence of Na2O, Cem. Concr. Res. 24 (1994) 563–572.

[49] W. Kunther, Z. Dai, J. Skibsted, Thermodynamic modeling of hydrated white Portland cement–metakaolin–limestone blends utilizing hydration kinetics from 29Si MAS NMR spectroscopy, Cem. Concr. Res. 86 (2016) 29–41.

[50] A. Machner, M. Zajac, M.Ben Haha, K.O. Kjellsen, M.R. Geiker, K.De Weerdt, Chloride-binding capacity of hydrotalcite in cement pastes containing dolomite and metakaolin, Cem. Concr. Res. 107 (2018) 163–181.

[51] C. Arya, N.R. Buenfeld, J.B. Newman, Factors influencing chloride-binding in concrete, Cem. Concr. Res. 20 (1990) 291–300.

[52] A. Delagrave, J. Marchand, J.-P. Ollivier, S. Julien, K. Hazrati, Chloride binding capacity of various hydrated cement paste systems, Adv. Cem. Based Mater. 6 (1997) 28–35.

[53] A. Vollpracht, B. Lothenbach, R. Snellings, J. Haufe, The pore solution of blended cements: a review, Mater. Struct. 49 (2016) 3341–3367.

[54] B. Lothenbach, K. Scrivener, R.D. Hooton, Supplementary cementitious materials, Cem. Concr. Res. 41 (2011) 1244–1256.

[55] S. Sui, W. Wilson, F. Georget, H. Maraghechi, H. Kazemi-Kamyab, W. Sun, K. Scrivener, Quantification methods for chloride binding in Portland cement and limestone systems, Cem. Concr. Res. 125 (2019), 105864.

[56] M.D. Andersen, H.J. Jakobsen, J. Skibsted, Characterization of the $\alpha - \beta$ phase transition in friedels salt (Ca2Al(OH)6Cl·2H2O) by variable-temperature 27Al MAS NMR spectroscopy, J. Phys. Chem. A 106 (2002) 6676–6682.

[57] G. Paul, E. Boccaleri, L. Buzzi, F. Canonico, D. Gastaldi, Friedel's salt formation in sulfoaluminate cements: a combined XRD and 27Al MAS NMR study, Cem. Concr. Res. 67 (2015) 93–102.

[58] M.D. Andersen, H.J. Jakobsen, J. Skibsted, A new aluminium-hydrate species in hydrated Portland cements characterized by 27Al and 29Si MAS NMR spectroscopy, Cem. Concr. Res. 36 (2006) 3–17.

[59] C.A.J. Appelo, The anion exchange properties of AFm (hydrocalumite-group) minerals defined from solubility experiments and crystallographic information, Cem. Concr. Res. 140 (2021), 106270.

[60] F. Georget, C. Bénier, W. Wilson, K.L. Scrivener, Chloride sorption by C-S-H quantified by SEM-EDX image analysis, Cem. Concr. Res. 152 (2022), 106656.

[61] S. Yoshida, Y. Elakneswaran, T. Nawa, Electrostatic properties of C-S-H and C-A-S-H for predicting calcium and chloride adsorption, Cem. Concr. Compos. 121 (2021), 104109.

[62] C. Labbez, A. Nonat, I. Pochard, B. Jönsson, Experimental and theoretical evidence of overcharging of calcium silicate hydrate, J. Colloid Interface Sci. 309 (2007) 303–307.

[63] S. Barzgar, M. Tarik, C. Ludwig, B. Lothenbach, The effect of equilibration time on Al uptake in C-S-H, Cem. Concr. Res. 144 (2021), 106438.

[64] D.A. Kulik, Improving the structural consistency of C-S-H solid solution thermodynamic models, Cem. Concr. Res. 41 (2011) 477–495.

[65] A.G. Kalinichev, J. Wang, R.J. Kirkpatrick, Molecular dynamics modeling of the structure, dynamics and energetics of mineral–water interfaces: application to cement materials, Cem. Concr. Res. 37 (2007) 337–347.

[66] D. Hou, Z. Li, Molecular dynamics study of water and ions transport in nano-pore of layered structure: a case study of tobermorite, Microporous Mesoporous Mater. 195 (2014) 9–20.